Characterizing the Ice-Ocean Interface of Icy Worlds: A Theoretical Approach

Jacob Buffo[1], B E Schmidt[2], C Huber[3], and C R Meyer[1]

[1]Dartmouth College
[2]Georgia Institute of Technology
[3]Brown University

November 24, 2022

Abstract

We investigate the structure and evolution of multiphase ice-ocean interfaces ('mushy layers') and the implications for the geophysics and habitability of ice-ocean worlds. Understanding the potential diversity of these multiphase layers across solar system bodies provides insight into the potential rates and mechanisms of heat and solute transport between their respective oceans and ice shells - which remain largely unconstrained. Additionally, variations in mushy layer properties may drive diverse geophysical processes unique to individual bodies or that may vary regionally on an individual icy world. We explore mushy layer evolution by analytically solving for the thickness of a simplified ice-ocean mushy layer system. We investigate two dynamic regimes, one driven by molecular diffusion and one driven by convection of brine within the mushy layer. We analyze the impact of gravity, thermal gradient, and ocean composition on the thickness of mushy layers. Additionally, a perturbation analysis is carried out to investigate the existence of mushy layer steady states. We show that stable mushy layers exist when ice shells are thickening, suggesting that mushy layers are likely persistent and common features of growing ice shells and accretionary regions of ice-ocean worlds.

Characterizing the Ice-Ocean Interface of Icy Worlds: A Theoretical Approach

J. J. Buffo[1], B. E. Schmidt[2], C. Huber[3], C. R. Meyer[1]
[1]Dartmouth College, [2]Georgia Institute of Technology, [3]Brown University

Abstract

We investigate the structure and evolution of multiphase ice-ocean interfaces ('mushy layers') and the implications for the geophysics and habitability of ice-ocean worlds. Understanding the potential diversity of these multiphase layers across solar system bodies provides insight into the potential rates and mechanisms of heat and solute transport between their respective oceans and ice shells - which remain largely unconstrained. Additionally, variations in mushy layer properties may drive diverse geophysical processes unique to individual bodies or that may vary regionally on an individual icy world. We explore mushy layer evolution by analytically solving for the thickness of a simplified ice-ocean mushy layer system. We investigate two dynamic regimes, one driven by molecular diffusion and one driven by convection of brine within the mushy layer. We analyze the impact of gravity, thermal gradient, and ocean composition on the thickness of mushy layers. Additionally, a perturbation analysis is carried out to investigate the existence of mushy layer steady states. We show that stable mushy layers exist when ice shells are thickening, suggesting that mushy layers are likely persistent and common features of growing ice shells and accretionary regions of ice-ocean worlds.

1 Introduction

Constraining the exchange of energy and mass between the oceans and ice shells of icy satellites in our solar system is crucial to understanding their geophysical evolution and assessing their habitability [*Jaumann et al.*, 2009; *Sotin and Tobie*, 2004; *Vance et al.*, 2018]. Likewise, in a rapidly changing Earth system, understanding and quantifying the interdependencies of the cryosphere, hydrosphere, atmosphere, and biosphere is imperative in constraining systems models aimed at providing accurate forecasts [*Notz*, 2012; *Notz and Bitz*, 2017]. In either case, the physics occurring near the ice-ocean interface play a disproportionate role. When ice forms from an aqueous solution, such as atop an ocean, it does not form a monocrystalline solid; rather, the ice-liquid interface is characterized by a porous matrix of dendritic (branching) ice crystals bathed in interstitial brine (e.g. Figure 1). Frequently referred to as a 'mushy layer', this two-phase regime forms a dynamic boundary which governs the evolution and properties of both the overlying ice and underlying water reservoir [*Buffo et al.*, *2020; Buffo et al.*, 2018; *Grumbine*, 1991; *Lake and Lewis*, 1970; *Lewis and Perkin*, 1983; *Turner and Hunke*, 2015; *Wells et al.*, 2019].

The most prevalent and well observed example of such an ice-ocean mushy layer is sea ice. While it has long been known that sea ice is a heterogeneous medium [*Malmgren*, 1927], only recently have the dynamics and effects of these physicochemical heterogeneities begun to be understood, quantified, and incorporated into numerical models. For sea ice, the mushy layer comprises a substantial amount of the ice cover and determines the heat and mass transport to and from both the ocean and atmosphere [*Aagaard and Carmack*, 1989; *Bitz and Lipscomb*, 1999; *Buffo et al.*, 2018; *Eicken et al.*, 2002; *Freitag*, 1999; *Griewank and Notz*, 2013; *Loose et al.*, 2009; *Loose et al.*, 2011; *Perovich et al.*, 1997; *Perovich et al.*, 2009; *Turner and Hunke*, 2015]. It provides an ecological niche for a diverse and important group of primary producers and grazers in the polar oceans [*Loose et al.*, 2011; *Tedesco and Vichi*, 2014; *Thomas and Dieckmann*, 2003; *Vancoppenolle et al.*, 2013; *Vancoppenolle and Tedesco*, 2015], plays a fundamental role in the formation of global ocean water masses [*Dickson and Brown*, 1994; *Grumbine*, 1991; *Hughes et al.*, 2014; *Robinson et al.*, 2014], and governs the properties and evolution of the overlying sea ice

[*Cottier et al.*, 1999; *Cox and Weeks*, 1974; *Eicken*, 1992; *Griewank and Notz*, 2015; *Kawano and Ohashi*, 2008; *Nakawo and Sinha*, 1981; *Ohashi*, 2007]. The evolution of this layer is best described by the equations of reactive transport in porous media, which account for the diffusive and advective transport of both heat and mass alongside thermochemical reactions [*Feltham et al.*, 2006; *Hunke et al.*, 2011]. Consequently, models which include the physics of multiphase reactive transport provide the most accurate simulations of sea ice growth, dynamics and material properties [*Bitz and Lipscomb*, 1999; *Griewank and Notz*, 2013; *Griewank and Notz*, 2015; *Wells et al.*, 2019; *Wells et al.*, 2011; *Wettlaufer et al.*, 1997a; *Worster and Rees Jones*, 2015].

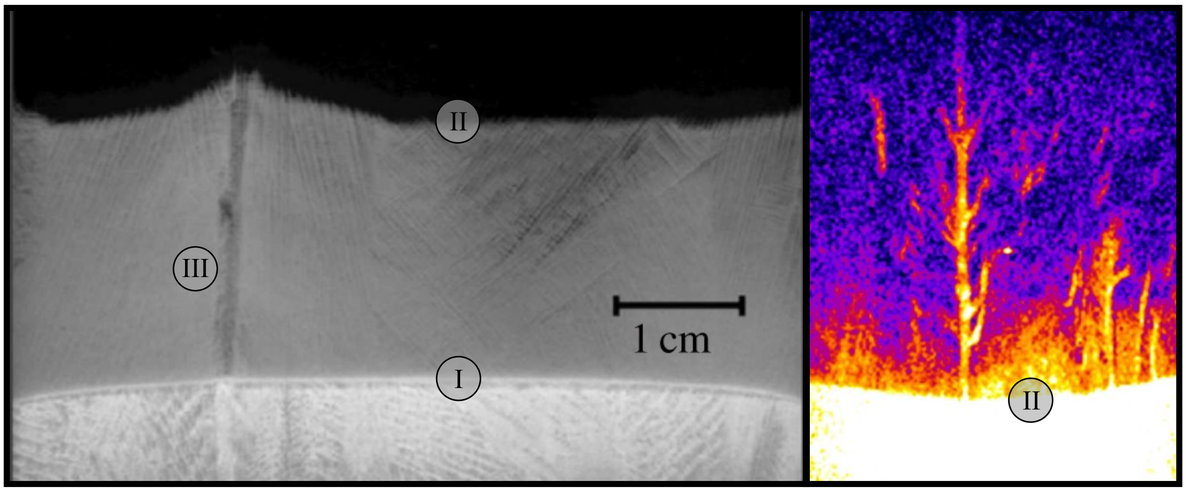

Figure 1 – Mushy layers in natural systems. (Left) A mushy layer forming from a 27 wt% ammonium chloride (NH_4Cl) solution cooled from below. (I) The solid-mush boundary marks the transition from a pure eutectic solid (bright white formation at the base of the image which has reached a temperature below the binary system solidification temperature (i.e. eutectic point)) to the mushy layer composed of both solid and liquid. (II) The mush-liquid boundary marks the transition from the mushy layer to the overlying pure fluid (dark region at the top of the image). (III) Density instabilities in the mushy layer, resulting from the chemical evolution of the pore fluid, drive convective processes which lead to the formation of channel structures – a common feature in mushy layer. Image modified from [*Zhong et al.*, 2012]. **(Right)** An MRI image of laboratory grown sea ice (top-down solidification). Light colors are associated with large liquid fractions and high salt concentrations. A positive gradient of both is clearly evident as the mush-liquid interface (II) is approached. For scale, the width of the image is 3.7 cm. Image modified from [*Worster and Rees Jones*, 2015].

Ice-ocean/brine interfaces are likely not a feature unique to Earth, as a number of other solar system bodies likely harbor substantial liquid water reservoirs [*Čadek et al.*, 2016; *Carr*, 1987; *Carr et al.*, 1998; *Kivelson et al.*, 2000; *Kuskov and Kronrod*, 2005; *Nimmo and Pappalardo*, 2016; *Porco et al.*, 2006; *Sohl et al.*, 2003; *Vance et al.*, 2014]. The putative structure of many of these ice-ocean worlds is a thick (2-80+ km) ice shell overlaying a subsurface ocean from which the ice shell likely formed (e.g. Europa, Triton, Enceladus) [*Schubert et al.*, 2004]. Other ice-ocean worlds (e.g. Callisto, Ganymede) may possess subsurface oceans thick enough to maintain layers of high-pressure ices separating their silicate interiors and liquid water reservoirs [*Fortes*, 2000; *Kuskov and Kronrod*, 2005; *Nagel et al.*, 2004; *Sohl et al.*, 2003; *Vance et al.*, 2014]. Triton and Pluto possess more exotic ices (e.g. ammonia, nitrogen) that may be in contact with subsurface oceans [*Gaeman et al.*, 2012; *Hammond et al.*, 2018; *Johnson et al.*, 2016; *Nimmo et al.*, 2016; *Robuchon and Nimmo*, 2011], while Ceres likely possesses a water-rich silicate crust and potentially a deep brine reservoir [*Castillo-Rogez and McCord*, 2010; *Ruesch et al.*, 2016] as well as localized near surface hydrological features beneath recent impact craters [*De Sanctis et al.*, 2016; *Hesse and Castillo-Rogez*, 2019; *Ruesch et al.*, 2016; *Schenk et al.*, 2019; *Scully et al.*, 2019]. The potentially widespread existence of ice-ocean/brine mushy layers, and their relation to the presence and persistence of liquid water, means constraining their dynamics and evolution has implications for geophysical processes and habitability across the solar system.

A feature that distinguishes the ice on all of these worlds from sea ice on Earth is its spatiotemporal scale. Sea ice is meters thick and ~1-10 years old, while the shells of icy satellites may be millions to billions of years old and are typically kilometers to tens of kilometers thick [*Hussmann et al.*, 2002; *Korosov et al.*, 2018; *Kurtz and Markus*, 2012; *Laxon et al.*, 2013; *Prockter*, 2017; *Schubert et al.*, 2004]. The orders of magnitude disparity between the spatial and temporal scales of sea ice and planetary ices likely indicates that the latter are subject to unique thermal and physicochemical processes that cannot be simulated wholescale in the laboratory or observed in terrestrial ices.

It has been suggested that these thick planetary ice layers may exhibit geophysical processes and stratigraphy akin to that of Earth's interior [*Barr and McKinnon*, 2007; *Head et al.*, 1997; *Kattenhorn and Hurford*, 2009; *Kattenhorn and Prockter*, 2014; *McKinnon*, 1999]. When the exterior ice shells of these worlds reach a critical thickness, they are thought to undergo solid-state convection, forming stratigraphic layers that mirror the terrestrial lithosphere-mantle-outer core system [*Barr and McKinnon*, 2007; *Foley and Becker*, 2009; *Head et al.*, 1997; *McKinnon*, 1999; *Mitri and Showman*, 2005]. The Galilean satellite Europa provides an archetype example of such a system, exhibiting surface geology indicative of a dynamic, layered ice shell [*McKinnon*, 1999], consisting of a brittle upper ice lithosphere (~2-6 km) [*Pappalardo and Coon*, 1996], a relatively isothermal, ductile ice mantle undergoing solid-state convection, overlaying a liquid water ocean (here, akin to Earth's outer core) [*Barr and McKinnon*, 2007; *McKinnon*, 1999; *Mitri and Showman*, 2005]. There exist regions where the icy lithosphere has likely been subducted/subsumed into the moon's interior [*Kattenhorn and Prockter*, 2014], surface features that suggest interaction with near surface water [*Manga and Michaut*, 2017; *Michaut and Manga*, 2014; *Schmidt et al.*, 2011], evidence of resurfacing [*Fagents et al.*, 2000; *Manga and Wang*, 2007], and dilational bands that mimic terrestrial mid-ocean ridges [*Head et al.*, 1999; *Howell and Pappalardo*, 2018; 2019; *Manga and Sinton*, 2004; *Prockter et al.*, 2002]. Moreover, the mottled texture and coloration of Europa's surface suggests there exist compositional and phase heterogeneities within the moon's ice shell [*Fanale et al.*, 1999; *Pappalardo and Barr*, 2004; *Zolotov and Shock*, 2001]. Much like the terrestrial rock cycle, physical and thermochemical variations within the ice shell likely play a crucial role in governing its material properties, dynamics and evolution [*Barr and McKinnon*, 2007; *Foley and Becker*, 2009; *Lyubetskaya and Korenaga*, 2007; *Steefel et al.*, 2005].

In the magmatic analog, melt transport and evolution, physicochemical heterogeneities, and regions of phase change are all important factors governing the interior geodynamics of Earth and the other terrestrial planets [*Foley and Becker*, 2009; *Lyubetskaya and Korenaga*, 2007; *Mckenzie*, 1984; *Nakagawa and Tackley*, 2004; *Reiners*, 1998; *Zhong et al.*, 2008]. Mushy layers dictate the thermochemical evolution of magma bodies [*Fowler*, 1987; *Huber et al.*, 2009; *Huber and Parmigiani*, 2018; *Mckenzie*, 1984] and the process of fractional crystallization can be extended to ice-ocean systems to understand the chemical evolution of interstitial brines. The terrestrial core-mantle boundary (CMB or D" region) is likely a molten mushy layer whose structure, topography, and dynamics may drive a number of global geophysical processes including plate tectonics, mantle plumes, and the geodynamo [*Burke et al.*, 2008; *Lay et al.*, 2008; *Maruyama et al.*, 2007; *Nakagawa and Tackley*, 2004; *Olson et al.*, 1987; *Olson et al.*, 2010]. This global solid-liquid interface likely exhibits density driven fluid processes and pressure dependent phase structure akin to the brine rejection and pressure induced basal accretion/ablation cycling of growing and evolving ice shells [*Buffo et al.*, *2020; Soderlund et al.*, 2014]. Thus, the analogous ice-ocean interface may play a similar role in driving the geodynamics of ice-ocean systems.

Including the physics associated with multiphase reactive transport processes has revolutionized geophysical models and drastically improved our understanding of Earth's interior and the surface expression of these subterranean dynamics [*Braun*, 2010; *Mckenzie*, 1984; *Steefel et al.*, 2005]. While ice-ocean worlds appear to undergo similar processing and exhibit a number of geological features consistent with a multiphase and hydrologically active lithosphere-mantle-ocean system [*Fagents et al.*, 2000; *Greeley et al.*, 2004; *Howell and Pappalardo*, 2018; *Kargel et al.*, 2000; *Kattenhorn and Prockter*, 2014; *Kuskov and Kronrod*, 2005; *Manga and Michaut*, 2017; *McKinnon*, 1999; *Michaut and Manga*, 2014; *Schmidt et al.*, 2011], the physical and thermochemical structure of these planetary ice layers remain largely unconstrained [*Buffo et al.*, *2020; Kargel et al.*, 2000]. A number of ice-ocean world geophysical models have highlighted the importance that impurities, heterogeneity, and melts may play in driving tectonism [*Howell and Pappalardo*, 2018; 2019; *Johnson et al.*, 2017], hydrological feature generation and evolution [*Manga and Michaut*, 2017; *Michaut and Manga*, 2014; *Schmidt et al.*, 2011], thermo-compositional convection in the ductile mantle [*Barr and McKinnon*, 2007], and the formation of geological features [*Head et al.*, 1999], however the majority of these models implement *a priori* heterogeneous distributions of salts and other impurities and do not incorporate the thermochemical evolution of multiphase systems explicitly. Conversely, recent work, e.g. [*Buffo et al.*, *2020; Hammond et al.*, 2018; *Hesse and Castillo-Rogez*, 2019; *Kalousová et al.*, 2014; 2016] has begun to demonstrate the crucial role reactive transport processes and properties of multiphase regions play in the dynamics and evolution of ice-ocean worlds. It is now clear that planetary ices are inhomogeneous and reactive: containing structural and chemical heterogeneities that determine their material properties, and in turn govern the characteristic geophysical processes on ice-ocean worlds.

A fundamentally important component in all of the systems outlined above is the multiphase boundary layer (mushy layer) between regions of solid and regions of liquid. Given the crucial role multiphase mushy layers play in terrestrial geophysical processes, investigating their likely analogous counterparts on ice-ocean worlds provides a novel window into potential ice shell processes. As a gateway for material and energy transport between the ocean and ice shell, mushy layers determine whether certain environmental parameters can act to catalyze or buffer material entrainment and/or heat transport at the ice-ocean interface. This has implications for ocean-surface material transport estimates, basally driven geodynamic processes, surface expression of potential ocean-derived biosignatures, as well as ice shell composition and material properties. Here, we present two such investigations; (1) the thickness and (2) the dynamic equilibrium sensitivity of mushy layers in diverse environments, and discuss the potential effects of small-scale multi-dimensional processes and heterogeneities (e.g. brine channels – Figure 1) on the properties and evolution of ice-ocean world mushy layers.

2 Derivation

Quantifying the dependence of mushy layer characteristics on local environmental pressures can aid in predicting the structure and dynamics of the potentially diverse mushy layers that may exist throughout the solar system, and how these variations could promote or constrain distinct geophysical processes. Here we investigate the thickness and stability of mushy layers using a simplified ice-mush-ocean system (Figure 2). (Note: all nomenclature used throughout the text can be found in Supplementary Section S2)

2.1 Equilibrium Mushy Layer Thickness

Given the geometry presented in Figure 2, we define the mushy layer thickness by two boundaries, the ice-mush interface (I – defined by a critical porosity, $\phi = \phi_c = 0.05$, which represents the percolation threshold of ocean-derived ices [*Golden et al.*, 2007]) and the mush-ocean interface (II – pure fluid boundary, $\phi = 1$). We assume that when the respective velocities of these two boundaries are equal an 'equilibrium' mushy layer of thickness *h* will form, i.e.:

$$v_m(t) = \dot{z}_m(t) = \dot{z}_m^*(t) = v_m^*(t) \tag{1}$$

We determine the velocity at each interface by solving two decoupled Stefan problems [*Huber et al.*, 2008; *Rubinšteĭn*, 2000; *Worster*, 1986], one dictated by heat transport, the other by mass (salt) transport. Such an approach is valid because at the mush-ocean interface (II), a high liquid fraction regime, a small change in liquid fraction (ice formation) will produce a certain amount of latent heat that needs to be removed from the interface before freezing can continue, while the resultant increase in salinity due to salt rejection from the forming ice will negligibly affect the freezing front propagation (i.e. at large liquid fractions the freezing point depression due to salinity increase will be small). Conversely, at the ice-mush interface (I), a low liquid fraction regime, an equal amount of latent heat will be produced by the same change in liquid fraction, but a much larger increase in salinity will occur due to salt rejection. Thus, the freezing point depression due to salinity increase will be large and for freezing to continue salt must be transported away from the interface. For example, let us assume perfect salt rejection from forming ice, a change in liquid fraction of 10%, and an initial pore fluid salinity of 50 ppt. At the mush-ocean interface a change in liquid fraction from 1 to 0.9 would increase the pore fluid salinity from 50 ppt to ~56 ppt. At the ice-mush interface a change in liquid fraction from 0.15 to 0.05 would increase the pore fluid salinity from 50 ppt to 150 ppt. While this is a simplification of a true planetary mushy zone, it captures the important features and lends itself to analytical solutions that bound the general evolution of the mushy layer. The strategy presented herein for solving these types of problems follows closely the heat transfer and Stefan problem solutions presented in *Turcotte and Schubert* [2014].

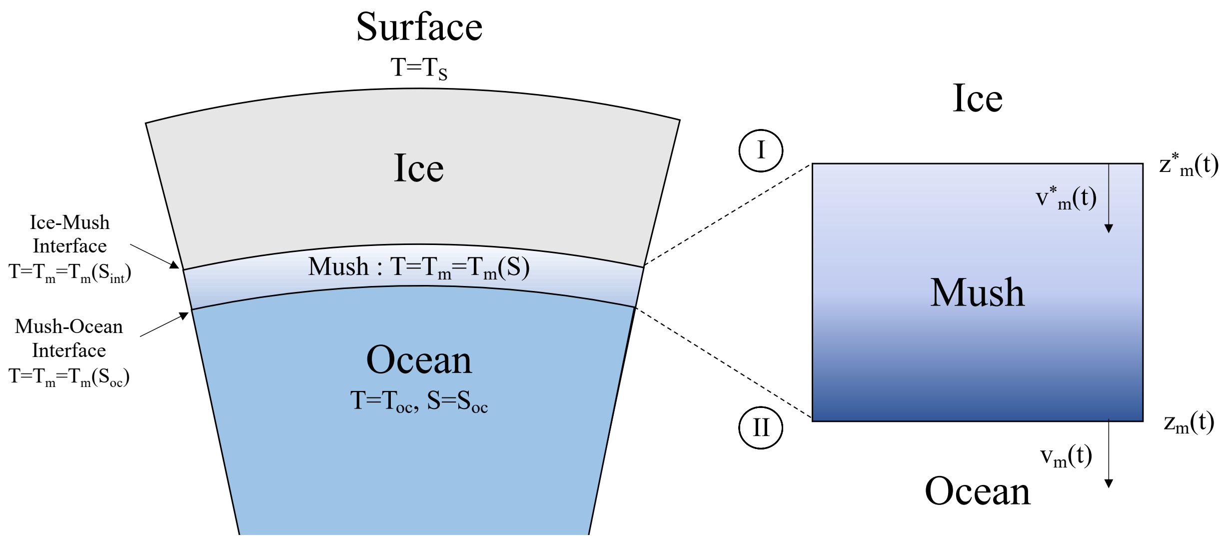

Figure 2 – Geometry and dynamics of the mushy layer. (Left) Schematic showing the simplified geometry of the ice-mush-ocean system as well as relevant boundary condition values. **(Right)** A magnified view of the mushy layer highlighting the ice-mush (I) and mush-ocean (II) interfaces and their respective propagation velocities. Color gradation in the mushy layer highlights the structural phase transition from low porosity ice to the pure fluid ocean. (Note: We consider a one-dimensional problem and assume that curvature is negligible as the distances we consider are much less than the radius of the body.)

We assume that the mush-ocean interface (interface II, $z_m(t)$) propagation is dictated by conductive heat transport away from the interface upwards through the overlying ice. This is the Stefan problem describing pure substance solidification and has the solution [*Huber et al.*, 2008; *Turcotte and Schubert*, 2014]:

$$z_m(t) = 2\lambda_T\sqrt{\kappa_i t} \tag{2}$$

$$\lambda_T \exp(\lambda_T^2) \operatorname{erf}(\lambda_T) = \frac{c_i(T_{oc} - T_S)}{L\sqrt{\pi}} \tag{3}$$

$$T(z,t) = T_S - (T_S - T_{oc})\frac{\operatorname{erf}\left(\frac{z}{2\sqrt{\kappa_i t}}\right)}{\operatorname{erf}(\lambda_T)} \tag{4}$$

Where $z_m(t)$ is the time dependent solidification front position, $T(z,t)$ is the time varying temperature profile in the overlying ice, λ_T is a transcendental variable, κ_i and c_i are the thermal diffusivity and specific heat of ice, T_{oc} and T_S are the ocean and surface temperature, respectively, and L is the latent heat of fusion for the water-ice phase transition.

We investigate the evolution of the ice-mush interface (interface I, $z_m^*(t)$) in two mass transport regimes: an advective regime when brine drainage is the dominant mechanism of salt transport and a diffusive regime when molecular diffusion is the dominant mechanism of salt transport. These two regimes provide endmember scenarios for mushy layer evolution: the advective regime will dominate the interface evolution of thin ice and ice-ocean/brine interfaces subject to large thermal gradients, while the diffusive regime will dictate the interface dynamics of thick and temperate ice [*Buffo et al., 2020*]. This is due to the need of a density instability to drive advection in the mushy layer. If ice formation is not rapid enough diffusion of salt away from the ice-mush interface should prevent such instabilities from forming [*Balmforth et al.*, 2007]. In either case, we will assume that there is no salt in the ice phase, and that the system is governed by the boundary conditions:

$$S(z = \infty, t) = S_{oc} \tag{5}$$

$$S(z = z_m^*(t), t) = S_{int} \tag{6}$$

$$S(z, t = 0) = S_{oc} \tag{7}$$

Where S_{oc} and S_{int} are the ocean and ice-mush interface salinity, respectively. Introducing the dimensionless salinity ratio:

$$\theta = \frac{S - S_{oc}}{S_{int} - S_{oc}} \tag{8}$$

We see that the boundary conditions on θ are:

$$\theta(z = \infty, t) = 0 \tag{9}$$

$$\theta(z = z_m^*(t), t) = 1 \tag{10}$$

$$\theta(z, t = 0) = 0 \tag{11}$$

2.1.1 Diffusion Regime

We investigate the interfacial velocity (and ultimately the mushy layer thickness) in the diffusive regime first. In this case, the evolution of salinity, S, in the system is governed by:

$$\frac{\partial S}{\partial t} = D\frac{\partial^2 S}{\partial z^2} \tag{12}$$

Where D is the molecular diffusivity of salt in water, here chosen to be constant so that it can be removed from the spatial derivative. In reality, ion diffusivity within porous media is a positively correlated function of porosity (e.g. Archie's Law [*Buffo et al.*, *2020; Buffo et al.*, 2018]). However, this will act to further limit ion mobility and thus does not alter our conclusions about mushy layer evolution in the diffusive regime. This problem is well documented in the literature [*Gewecke and Schulze*, 2011a; b; *Worster*, 1986], and we include the detailed solution of Equation 12 and the resulting mushy layer equilibrium thickness equations for the specific geometry outlined in Figure 2 in Supplementary Section S1.

In this diffusive regime, equilibrium mushy layer thicknesses always exceed the total ice thickness (Supplementary Equation S12 & S13). This is an impossible mushy layer thickness and implies that there does not exist stable mushy layer thicknesses driven by diffusion of salt from the ice-mush interface. This is a known result for mushy layers growing in an infinite half space [*Worster*, 1986] as the molecular diffusivity of salt is much less than the thermal diffusivity of ice (Lewis number $= Le = \kappa_i/D \gg 1$) and salinity is tied to temperature by a linear liquidus relationship (concentration dependent freeing point - see Equation S11 or Equation 24). Thus, large salinity gradients in the absence of large thermal gradients cannot occur (which could potentially offset the difference between D and κ_i), and ice growth at the mush-ocean interface outpaces salt diffusion at the ice-mush interface.

2.1.2 Advection Regime

When advection dominates diffusion, the evolution of salinity in the system is governed by:

$$\frac{\partial S}{\partial t} = -b\frac{\partial S}{\partial z} \tag{13}$$

Where b is the brine velocity out of the interfacial layer parameterized by the Rayleigh number dependent linear relationship presented in [*Griewank and Notz*, 2013] (See Equation 22). In dimensionless form θ:

$$\frac{\partial \theta}{\partial t} = -b\frac{\partial \theta}{\partial z} \tag{14}$$

We introduce the dimensionless length scale:

$$\eta = \frac{z}{bt} \tag{15}$$

And it follows that at the interface, z_m^*, the dimensionless variable can be written:

$$\eta_m = \frac{z_m^*}{bt} \tag{16}$$

Rewriting the advection equation components in terms of η:

$$\frac{\partial \theta}{\partial t} = \frac{d\theta}{d\eta}\frac{\partial \eta}{\partial t} = \frac{d\theta}{d\eta}\frac{-z}{bt^2} = -\frac{\eta}{t}\frac{d\theta}{d\eta} \tag{17}$$

$$\frac{\partial \theta}{\partial z} = \frac{d\theta}{d\eta}\frac{\partial \eta}{\partial z} = \frac{1}{bt}\frac{d\theta}{d\eta} \tag{18}$$

$$\Rightarrow \ \eta\frac{d\theta}{d\eta} = \frac{d\theta}{d\eta} \tag{19}$$

Therefore $\eta = \eta_m = 1$. Which implies that:

$$z_m^* = bt \tag{20}$$

In this way, we demonstrate that the interface will propagate as fast as salt can be advected away from it. Setting the two velocities equal to each other ($\dot{z}_m(t) = \dot{z}_m^*(t)$, Equation 1) and solving for *h,* we make use of the one-dimensional gravity drainage parameterization of *Griewank and Notz* [2013], which describes the convective overturn of brine in the mushy layer, and the relationship between thermal gradient and freezing front propagation velocity that can be garnered from the solution to the classic thermal Stefan problem (See Eq. 2-4 and [*Buffo et al.*, *2020*]). $\dot{z}_m^*(t) = b = v_m(t) = \dot{z}_m(t)$, from *Buffo* [2019]:

$$v_m(t) = -\frac{\partial T}{\partial z}\frac{\operatorname{erf}(\lambda_T)\sqrt{\pi}\lambda_T\kappa_i\exp(\lambda_T^2)}{(T_S - T_{oc})} \tag{21}$$

And from [*Griewank and Notz*, 2013]:

$$b = \alpha\left(\frac{g\rho_{sw}\beta\Delta S\Pi h}{\kappa_{br}\mu} - Ra_c\right) \tag{22}$$

Where α is a coefficient describing the linear relationship between brine drainage and the local Rayleigh number ($Ra = g\rho_{sw}\beta\Delta S\Pi h/\kappa_{br}\mu$), g is gravity, ρ_{sw} is ocean density, β is the solute contraction coefficient, ΔS is the difference in salinity between the interface and the ocean, $S_{int} - S_{oc}$, Π is the minimum permeability of the mushy layer, κ_{br} is the thermal diffusivity of the brine, μ is kinematic viscosity, and Ra_c is the critical Rayleigh number of the mushy layer. Assuming a conductive (linear) thermal profile in the ice shell, $\partial T/\partial z = (T_{oc} - T_S)/H$, we have:

$$\alpha\left(\frac{g\rho_{sw}\beta\Delta S\Pi h}{\kappa_{br}\mu} - Ra_c\right) = \frac{\operatorname{erf}(\lambda_T)\sqrt{\pi}\lambda_T\kappa_i\exp(\lambda_T^2)}{H} \tag{23}$$

We assume that the interface is at its melting temperature, T_f, which we take as a linear function of salinity $T_f = T_{mp} - \Gamma S$, where T_{mp} is the melting temperature of pure ice and the freezing point depression coefficient, Γ, is taken to be 0.066178 K kg g^{-1}. Solving for S and letting T_f lie on the conductive thermal profile $T(z) = T_S + z(T_{oc} - T_S)/H$ at a depth *H-h*. We have:

$$S_{int} = \Gamma^{-1}(T_{mp} - T_f) = \Gamma^{-1}\left\{T_{mp} - \left[T_S + (H-h)\frac{(T_{oc} - T_S)}{H}\right]\right\} \tag{24}$$

Substituting S_{int} into ΔS:

$$\alpha\left\{\frac{g\rho_{sw}\beta\left[\Gamma^{-1}\left(T_{mp} - \left\{T_S + (H-h)\frac{(T_{oc} - T_S)}{H}\right\}\right) - S_{oc}\right]\Pi h}{\kappa_{br}\mu} - Ra_c\right\} = \frac{\operatorname{erf}(\lambda_T)\sqrt{\pi}\lambda_T\kappa_i\exp(\lambda_T^2)}{H} \tag{25}$$

This is the key equation for calculating mushy layer thickness as a function of the environmental parameters of the system. Algebraic manipulation reveals this equality produces a quadratic equation in h with one positive root and one negative root (which can be ignored, as a negative mushy layer thickness is not physically meaningful). Equation 25 is the product of a velocity balance between the upper and lower boundaries of a simplified ice-ocean interface mushy layer and describes the evolving mushy layer thickness as the overlying ice column evolves. Our derivation and resulting equation for mushy layer thickness mirrors contemporary approaches to solving rudimentary ice-ocean mushy layer problems (e.g. [*Balmforth et al.*, 2007]) and our first principles approach makes it broadly applicable to any ice-ocean interface, terrestrial or planetary. Lastly, the permeability-porosity relationship utilized is that of [*Griewank and Notz*, 2013], which gives:

$$\Pi = \Pi(\phi = \phi_c) = K_0 \phi^{\gamma} \tag{26}$$

Where K_0 is a characteristic permeability (here $1.99526 \times 10^{-8}\ m^2$), and γ is a dimensionless coefficient relating permeability and porosity (here taken to be 3.1). It is important to note that in the derivation of Equation 25, and throughout the text, permeability is calculated using the critical porosity of the ice-mush interface. While certainly a simplification in the inherently heterogeneous mushy layer, porosity gradients are at a minimum near the ice-mush interface [*Buffo et al.*, 2018] and such a pseudo-analytical approach allows us to place novel constraints on the structure of an important and likely ubiquitous geophysical interface. To first order, we solve for the expected mushy layer thickness under given environmental conditions and provide a method to predict and compare the general characteristics and evolution of multiphase interfaces across different ice-ocean worlds in the solar system.

3 Results

To investigate the influence of a number of environmental parameters on the equilibrium thickness of mushy layers we solve Equation 25 under variable gravity, ocean composition, and thermal forcing. The intention of this parametric study is to understand the range of potential mushy layer properties and corresponding dynamics that may arise across the diverse ice-ocean worlds that populate our solar system. We carry out a perturbation analysis, demonstrating that these equilibrium thicknesses are indeed stable. Finally, we discuss potential implications of variable mushy layer thicknesses on the habitability, geophysics, and future spacecraft observations of ice-ocean worlds.

3.1 Validation Under Terrestrial Conditions

It is instructive to compare the mushy layer equilibrium thicknesses predicted by Equation 25 for the terrestrial ice-ocean system to existing laboratory and field measurements. Assuming a terrestrial ocean composition (Supplementary Section S3), we investigate three surface temperatures; 230 K, 265 K, and 270 K, for an ocean temperature of 270.90 K (just slightly above its liquidus temperature of 270.88 K – see Γ of Table 1). The relationship between ice thickness (*H*) and mushy layer equilibrium thickness (*h*) for all three surface temperatures can be seen in Figure 3, demonstrating that colder surface temperatures promote thinner equilibrium mushy layer thicknesses. Mushy layer equilibrium thicknesses range between 0-10 cm. These thicknesses agree well with values measured in both laboratory experiments of sea ice growth [*Wettlaufer et al.*, 1997a; b] and empirical observation of natural sea ice [*Notz and Worster*, 2008], which typically find mushy layer thicknesses ~10 cm. Sea ice is relatively thin and thus supports substantial thermal gradients [~10 K/m] when compared to those near the base of terrestrial ice shelves [~0.08 K/m [*Zotikov et al.*, 1980]] and those expected at the base of planetary ice shells [~0.02 K/m [*McKinnon*, 1999; *Mitri and Showman*, 2005]], resulting in relatively thin equilibrium mushy layer thicknesses. Thicker ice with lower interfacial thermal gradients should support thicker mushy layers, and indeed columnar ice accreted 410 m beneath the Ross Ice Shelf was observed to be hydraulically connected to the underlying ocean multiple meters above the ice-ocean interface

[*Zotikov et al.*, 1980]. These results can be reconciled by understanding that the ice-mush interface will be at its liquidus melting point (Equation 24) and that the conduction driven temperature profile in the ice will be approximately linear [*Buffo et al.*, 2018; *Buffo et al.*, *2020*]. For colder surface temperatures or thinner ice, a given liquidus temperature will lie closer to the mush-ocean interface than it would under warmer surface temperatures or in thicker ice, respectively, producing thinner mushy layers.

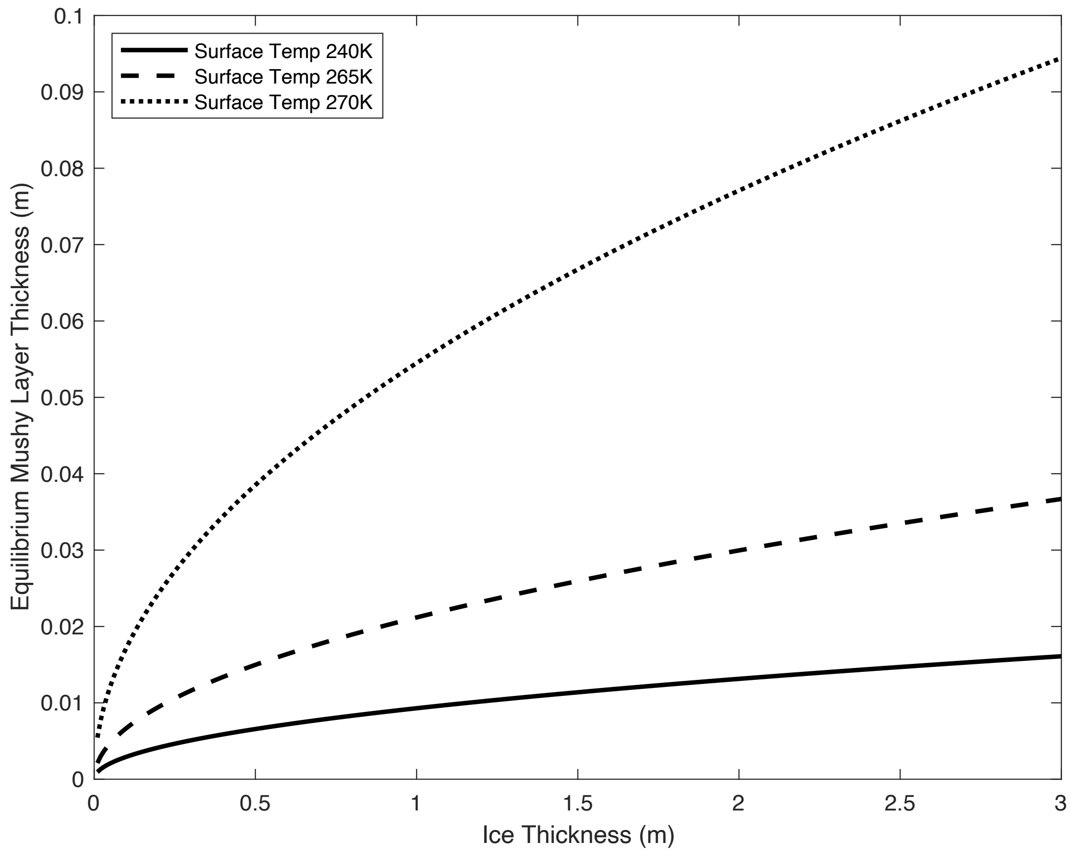

Figure 3 – Terrestrial mushy layer equilibrium thicknesses. As ice-ocean interface thermal gradients decrease equilibrium mushy layer thickness increases. These results match empirical observations of terrestrial ices, both qualitatively and quantitatively, as newly formed ice typically supports thin mushy layers that thicken with growth of the ice cover, reaching thicknesses ~10 cm.

3.2 Default Parameters

In the following sections (3.3-3.5) we investigate the dependence of mushy layer equilibrium thickness on a number of environmental parameters. Unless otherwise stated, the values utilized in the solution of Equation 25 are those given in Table 1.

Variable	Value
$\boldsymbol{\kappa_i}$	$1.09 \times 10^{-6}\ \mathrm{m^2\ s^{-1}}$
$\boldsymbol{\kappa_{br}}$	$1.48 \times 10^{-7}\ \mathrm{m^2\ s^{-1}}$
$\boldsymbol{c_i}$	$2000\ \mathrm{J\ kg^{-1}\ K^{-1}}$

$\boldsymbol{L}$	$334{,}774\ \mathrm{J\ kg^{-1}}$
$\boldsymbol{\alpha}$	$1.56 \times 10^{-1}\ \mathrm{kg\ m^{-3}\ s^{-1}}$
$\boldsymbol{g}$	$1.32\ \mathrm{m\ s^{-2}}$
$\boldsymbol{\rho_{sw}}$	$1027.347\ \mathrm{kg\ m^{-3}}$
$\boldsymbol{\beta}$	$5.836 \times 10^{-4}\ \mathrm{ppt^{-1}}$
$\boldsymbol{\kappa}$	$1.47 \times 10^{-7}\ \mathrm{m^2\ s^{-1}}$
$\boldsymbol{\mu}$	$1.88 \times 10^{-3}\ \mathrm{m^2\ s^{-1}}$
$\boldsymbol{\Pi}$	$^{\dagger}1.848 \times 10^{-12}\ \mathrm{m^2}$
$\boldsymbol{\Gamma}$	6.6178×10^{-2} K kg g^{-1}
$\boldsymbol{T_S}$	100 K
$\boldsymbol{T_{oc}}$	270.90 K
$\boldsymbol{S_{oc}}$	34 ppt
$\boldsymbol{T_{mp}}$	273.15 K
$\boldsymbol{T_f}$	$(T_{mp} - \Gamma \mathrm{S})$ K
$\boldsymbol{Ra_c}$	1.01×10^{-2}
Ocean Composition	Terrestrial (Supplementary Section S3)

Table 1 – Representative values for the Europa system. †Permeability calculated via the permeability-porosity relationship of *Griewank and Notz* [2013] (Equation 26) using a critical porosity of 0.05.

3.3 Gravity

To investigate the effects of gravity on mushy layer equilibrium thickness we solve Equation 25 using conditions for Earth ($g = 9.8\ \mathrm{m/s^2}$), Europa ($g = 1.315\ \mathrm{m/s^2}$), and Enceladus ($g = 0.113\ \mathrm{m/s^2}$). The relationship between ice shell thickness (*H*) and mushy layer equilibrium thickness (h) for all three gravities can be seen in Figure 4, which shows that ice-ocean worlds with lower gravity can support much thicker mushy layers. This is a logical result, as the density instability driving advective transport of brine within the mushy layer and away from the ice-mush interface is proportional to gravity (Equation 22). Thus, on worlds with lower gravity, thicker mushy layers are required to produce the same magnitude of convective overturn (gravity drainage [*Griewank and Notz*, 2013]). Variations in mushy layer thickness will impact the rate and method of heat and solute transport to and from the underlying ocean, affecting ice shell growth rates as well as the thermochemical characteristics and evolution of the ice that forms. Additionally, the stable thickness of the mushy layer will determine the extent of hydraulic conductivity within the lower layer of the ice shell, constraining the penetration height above the mush-ocean interface where substantially connected pore fluid could potentially exist. This has important implications for relating chemical measurements of plume particles to their origin sources. Plumes have repeatedly been associated with the expression of subsurface water reservoirs [*Porco et al.*, 2006; *Sparks et al.*, 2016]. However, a plume sourced by highly concentrated/modified pore fluid within the shell (e.g. the interstitial fluid near the ice-mush interface as opposed to directly from the ocean) could substantially alter interpretation of the interior ocean composition [*Hansen et al.*, 2011; *Postberg et al.*, 2009; *Postberg et al.*, 2011].

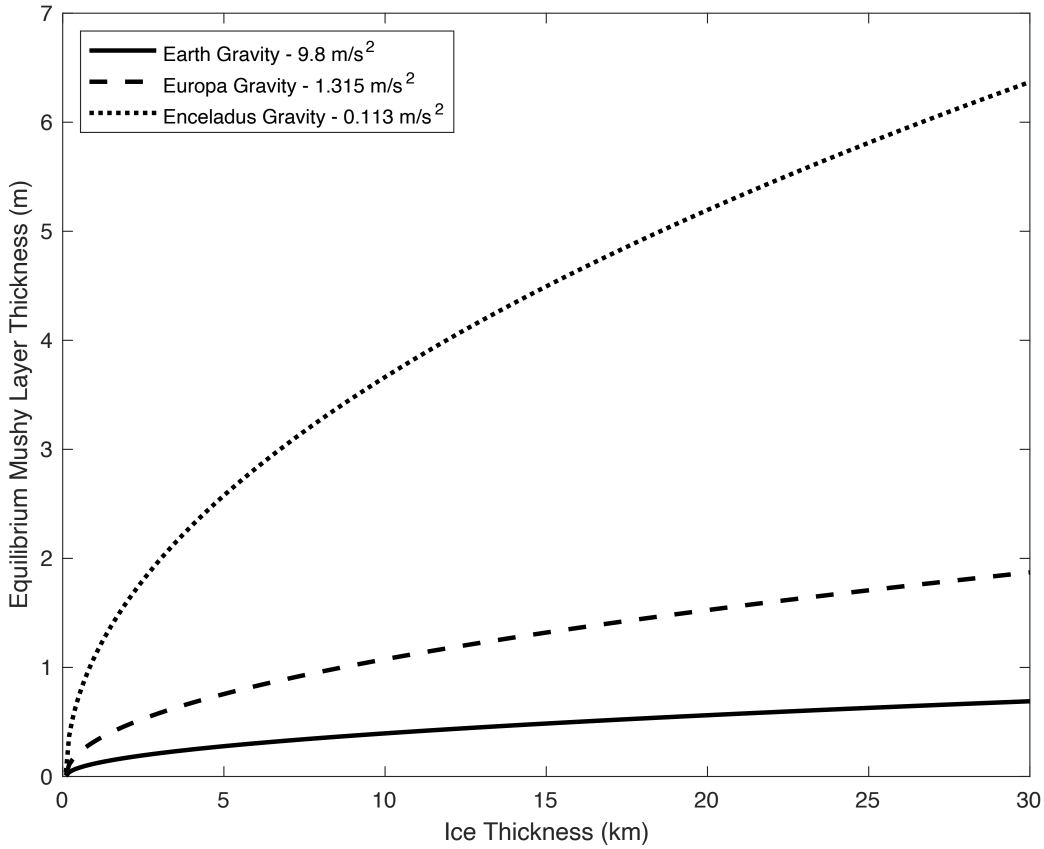

Figure 4 – Mushy layer equilibrium thickness vs. ice shell thickness under variable gravity. Bodies with lower gravity support mushy layers of greater thickness. This is a direct consequence of the dependence of pore fluid convection on local density instabilities. Substantial mushy layers on smaller bodies (e.g. Enceladus) may promote ice-ocean heat and solute transport dynamics that differ from those of their larger counterparts (e.g. Earth, Europa).

3.4 Ocean Composition

To investigate the effects of ocean composition on the equilibrium thickness of the mushy layer we solve Equation 25 using a modified solute contraction coefficient ($\beta \rightarrow 0.5\beta$) and an alternate freezing point depression equation ($T_f = T_{mp} - 0.5\Gamma S$). The physical significance of altering the solute contraction coefficient is to investigate how lower density salts will affect the properties of the mushy layer. Similarly, altering the freezing point depression equation will elucidate how a salt which has less of an effect on the liquidus of the solution will alter the characteristics of the mushy layer (e.g. $MgSO_4$ compared to NaCl). We assume an ocean concentration of 34 ppt and utilize an ocean temperature equal to the freezing point of the respective ocean, while the surface temperature was set to 170 K below the ocean temperature (for consistent thermal gradients). Additionally, for the simulation with an alternate density coefficient we reduced the ocean density to reflect the presence of the lower density salt ($\rho_{sw} = 1013.67\ \mathrm{kg/m^3}$). The relationship between ice shell thickness (H) and mushy layer equilibrium thickness (h) for the modified systems, as well as that for an unmodified ocean, can be seen in Figure 5. Reducing the density of the solute results in thicker equilibrium mushy layer thicknesses. This is reasonable to expect as thicker mushy layers are required to produce the density instabilities needed to drive gravity drainage when lower density salts are present (the dependence of Equation 22 on β). Conversely, solutes which depress the freezing point of the solution less than the control result in thinner equilibrium mushy layer thicknesses. This is also expected, as less extreme temperatures are needed to concentrate the pore fluid and induce brine drainage (equivalent to the relocation of the ice-mush interface liquidus point closer to the mush-ocean interface as discussed in Section 3.1). This suggests that ocean composition may play a substantial role in governing the physical properties and dynamics of ice-ocean interfaces.

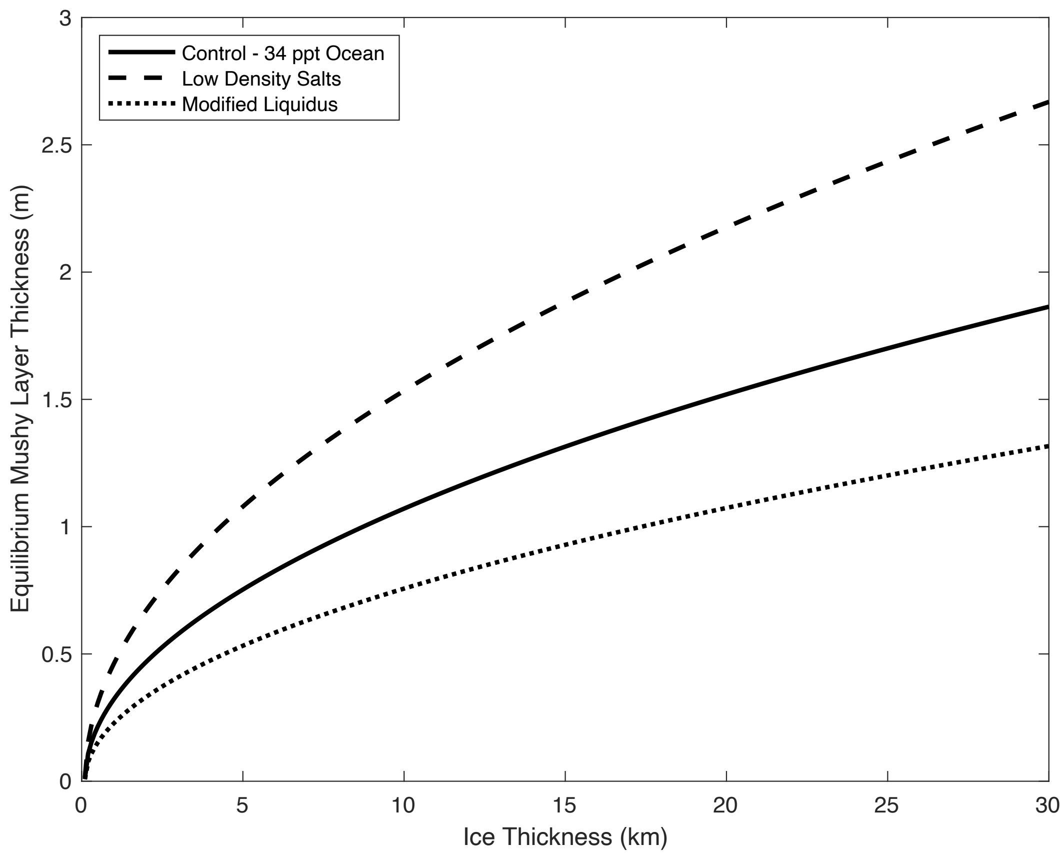

Figure 5 – Mushy layer equilibrium thickness vs. ice shell thickness for variable ocean compositions. Low density solutes increase the equilibrium mushy layer thickness, while solutes with less freezing point depression capabilities ('Modified Liquidus') result in thinner equilibrium mushy layer thicknesses.

3.5 Thermal Gradient

To investigate the effects of ice-ocean thermal gradient on the equilibrium thickness of the mushy layer we solve Equation 25 using three surface temperatures; 35 K, 100 K, and 230 K. This is an implicit alteration to the thermal gradient $\partial T/\partial z = (T_{oc} - T_S)/H$, as this is the only occurrence of T_S in the simplified form of Equation 25 (See Equations 36 & 37). The relationship between ice shell thickness (H) and mushy layer equilibrium thickness (h) for the various thermal gradients can be seen in Figure 6. The curves show that decreased thermal gradients at the ice-ocean interface support much thicker equilibrium mushy layer thicknesses. This is a logical consequence of assuming local thermodynamic equilibrium in the mushy layer. With the mush salinity tied to the liquidus (Equation 24), a thicker mushy layer must be formed to produce the same local Rayleigh number (Equation 22), and thus ice-mush interface velocity, for a smaller thermal gradient than would be needed to produce the same ice-mush interface velocity under a larger thermal gradient. This is important as the large scale of planetary ice shells, along with the potential for ongoing intrashell hydrologic activity, suggests that different regions within the ice shell have been subject to a diverse range of thermal gradients over their long history, providing a mechanism which could introduce heterogeneities in the physicochemical characteristics of the ice shell.

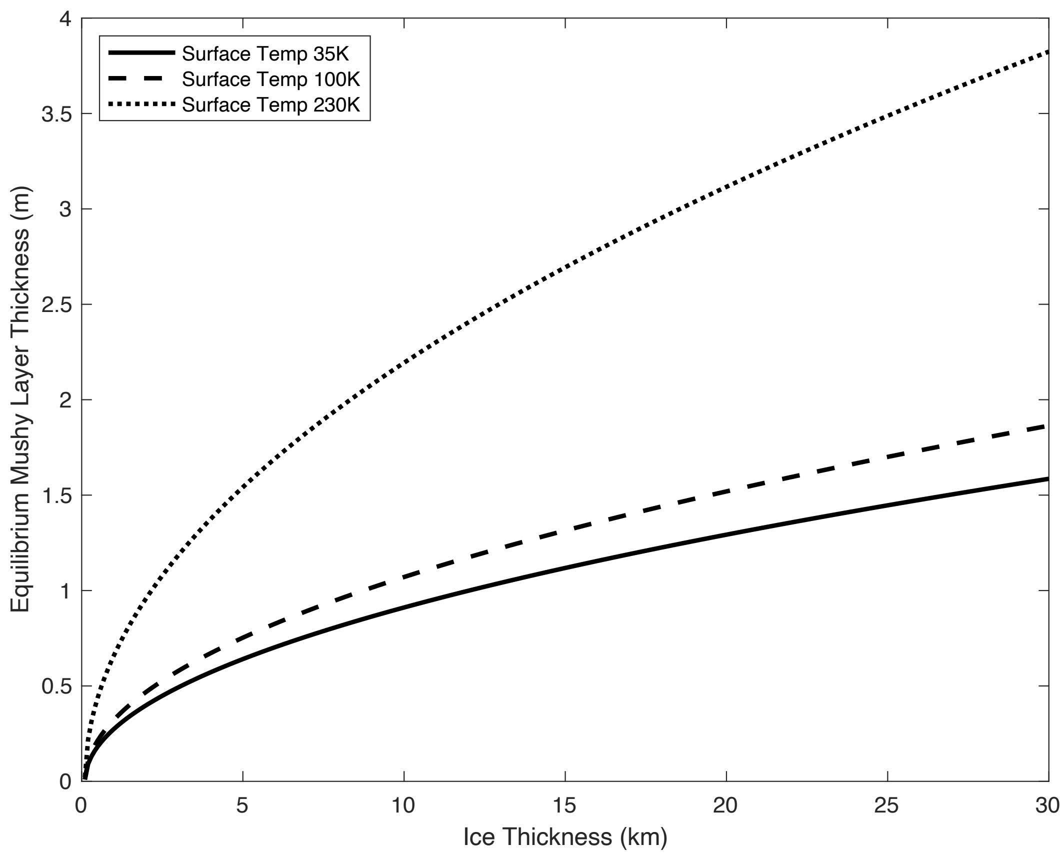

Figure 6 – Mushy layer equilibrium thickness vs. ice shell thickness under variable ice-ocean interface thermal gradient. As ice-ocean thermal gradients decrease equilibrium mushy layer thickness increases. Similar to the terrestrial case (Figure 3), this suggests that the ice-ocean interfaces of thick ice shells should be characterized by substantially thick, hydraulically connected, multiphase layers – allowing for ongoing fluid and solute transport. Such a layer could promote the formation and sustenance of interstitial chemical gradients favorable for potential organisms as well as constitute a unique and spatiotemporally variable medium for heat exchange between the ocean and ice shell (e.g. [*Soderlund et al.*, 2014]).

3.6 Mushy Layer Sensitivity

It is important to quantify the stability of the ice-ocean interface mushy layer of icy worlds to determine if these boundaries are long-lived and stable components of ice shells or exist as transient features. As evidenced by their terrestrial counterparts, the dynamics and evolution of these boundary layers determine the growth rate and physicochemical composition of the overlying ice [*Eicken*, 1992; *Nakawo and Sinha*, 1981; *Wolfenbarger et al.*, 2018; *Zotikov et al.*, 1980]. The disparity between the material properties of ocean-derived ices that form in different conditions on Earth (e.g. sea ice vs. marine ice), alongside expected heterogeneities in ocean circulation, ice shell thickness, and surface temperature on ocean worlds [*Ojakangas and Stevenson*, 1989; *Soderlund*, 2019; *Soderlund et al.*, 2014], suggests that these bodies likely support a spectrum of ice-ocean interface conditions resulting in potentially diverse ices. Regional heterogeneities in ice properties could power geophysical processes [*Barr and McKinnon*, 2007] and facilitate inhomogeneous ocean-surface material transport.

It is therefore instructive to determine the response and resilience of mushy layers to variations in internal properties and environmental conditions. To investigate the stability of the mushy layer we will assume the system is in equilibrium, perturb it by a small amount, and study the effect it has on the difference in velocity between the two fronts $\Delta V = v_m(t) - v_m^*(t)$. It is important to note that $\Delta V = 0$ for equilibrium mushy layer thicknesses, $\Delta V < 0$ for thinning mushy layers, and $\Delta V > 0$ for thickening mushy layers. We will investigate two types of perturbations: perturbations to mushy layer thickness, h' ($h \rightarrow h + h'$), and perturbations to thermal gradient, G' ($(T_{oc} - T_S)/H = \partial T/\partial z = G \rightarrow G + G'$). These parameters were selected as they encapsulate the potentially dynamic thermophysical properties of realistic ice-mush-ocean systems that influence ice-mush and mush-ocean interface velocities, and thus mushy layer thicknesses (e.g. ocean temperature, surface temperature, ice shell thickness, mushy layer thickness). Above we've shown that for the advective regime the mush-ocean interface velocity is:

$$v_m(t) = \frac{(T_{oc} - T_S)\kappa_i c_i}{HL} \qquad (27)$$

And the ice-mush interface velocity is:

$$v_m^*(t) = \frac{\alpha g \rho_{sw} \beta (\Gamma^{-1} \left(T_{mp} - T_S + (h - H)\frac{(T_{oc} - T_S)}{H} \right) - S_{oc}) \tilde{\Pi} h}{\kappa \mu} - \alpha Ra_c \qquad (28)$$

For perturbations to the equilibrium mushy layer thickness, $h \rightarrow h + h'$, $v_m(t)$ is unchanged if H is fixed. For $v_m^*(t)$ let $C_1 = \alpha g \rho_{sw} \beta \tilde{\Pi} / \kappa\mu$, then:

$$v_m^*(t, h \rightarrow h + h') = C_1 (h + h')(\Gamma^{-1} \left(T_{mp} - T_S + ((h + h') - H)\frac{(T_{oc} - T_S)}{H} \right) - S_{oc}) - \alpha Ra_c \qquad (29)$$

$$= \left[C_1 h \Gamma^{-1} \left(T_{mp} - T_S + (h - H)\frac{(T_{oc} - T_S)}{H} \right) - S_{oc}) - \alpha Ra_c \right]$$
$$+ \left[C_1 h h' \Gamma^{-1} \frac{(T_{oc} - T_S)}{H} + C_1 h' (\Gamma^{-1} \left(T_{mp} - T_S + ((h + h') - H)\frac{(T_{oc} - T_S)}{H} \right) - S_{oc}) \right] \qquad (30)$$

Where the terms in the first set of square brackets are just the original interface velocity due to the equilibrium mushy layer thickness h, and the terms in the second set of square brackets are the change in interface velocity due to the perturbation h', we'll call this Δv_m^*:

$$\Delta v_m^* = C_1 h h' \Gamma^{-1} \frac{(T_{oc} - T_S)}{H} + C_1 h' \left(\Gamma^{-1} \left(T_{mp} - T_S + ((h + h') - H)\frac{(T_{oc} - T_S)}{H} \right) - S_{oc} \right) \qquad (31)$$

$$= C_1 h h' \Gamma^{-1} \frac{(T_{oc} - T_S)}{H} + C_1 h' \left(\Gamma^{-1} \left(T_{mp} - T_S + (h - H) \frac{(T_{oc} - T_S)}{H} \right) - S_{oc} \right)$$
$$+ C_1 h' h' \Gamma^{-1} \frac{(T_{oc} - T_S)}{H} \qquad (32)$$

Linearizing:

$$\Delta v_m^* \approx C_1 h h' \Gamma^{-1} \frac{(T_{oc} - T_S)}{H} + C_1 h' \left(\Gamma^{-1} \left(T_{mp} - T_S + (h - H) \frac{(T_{oc} - T_S)}{H} \right) - S_{oc} \right) \qquad (33)$$

For the first term on the right-hand side, $C_1 h \Gamma^{-1} \frac{(T_{oc} - T_S)}{H} \geq 0$ for all realistic values of C_1, h, H, Γ and assuming the ice is thickening i.e. $T_{oc} > T_S$, which is the case we consider here. For the second term on the right-hand side, $C_1 \left(\Gamma^{-1} \left(T_{mp} - T_S + (h - H) \frac{(T_{oc} - T_S)}{H} \right) - S_{oc} \right) = C_1 (S_{int} - S_{oc}) \geq 0$ for all realistic values of C_1 and assuming $S_{int} > S_{oc}$, which is reasonable for thickening ice. Substituting into the definition of ΔV gives:

$$\Delta V = v_m(t) - v_m^*(t, h \rightarrow h + h') = v_m(t) - (v_m^*(t) + \Delta v_m^*) = -\Delta v_m^* \qquad (34)$$

Thus,

$$\begin{cases} \Delta V < 0 & if \quad h' > 0 \\ \Delta V > 0 & if \quad h' < 0 \end{cases} \qquad (35)$$

This suggests that if the mushy layer thickens ($h' > 0$), the ice-mush interface velocity will increase, thinning the mushy layer, while if the mushy layer thins ($h' < 0$) the ice-mush velocity will decrease, thickening the mushy layer. Furthermore, $\Delta V \propto \Delta v_m^* \propto h' + h'^2$ (Equation 32), thus $\Delta V \rightarrow 0$ smoothly as $h' \rightarrow 0$. This implies that the mushy layer thickness *h* is a stable equilibrium, i.e. perturbations from this equilibrium thickness will decay (be smoothed out by the system).

It is additionally instructive to investigate how the system will respond to variations in environmental parameters (e.g. T_S, T_{oc}, and H). This is important as a number of geophysical phenomena could potentially alter the ice-ocean interface environment. For example; regional/global ocean warming/cooling events [*Goodman and Lenferink*, 2012; *Melosh et al.*, 2004; *Soderlund et al.*, 2014], thickening of the overlying ice shell by surface deposition [*Fagents*, 2003; *Fagents et al.*, 2000] or the intrusion of hydrologic features within the shell [*Manga and Michaut*, 2017; *Michaut and Manga*, 2014]. To investigate the stability of mushy layers to variations in environmental parameters we will explore how ΔV behaves when subject to small perturbations in thermal gradient, G' ($(T_{oc} - T_S)/H = \partial T/\partial z = G \rightarrow G + G'$). Here G' is a constant shift in thermal gradient.

Rewriting Equations 27 and 28 in terms of thermal gradient ($G = \partial T/\partial z = (T_{oc} - T_S)/H$) gives:

$$v_m = G \frac{\kappa_i c_i}{L} \qquad (36)$$

$$v_m^* = C_1 h \left[\Gamma^{-1} \left(T_{mp} - (T_{oc} - hG) \right) - S_{oc} \right] - \alpha Ra_c \qquad (37)$$

Introducing a perturbation to the thermal gradient ($G \rightarrow G + G'$):

$$v_m \to v_m + G' \frac{\kappa_i c_i}{L} \quad (38)$$

where $\Delta v_m = G' \kappa_i c_i / L$, and

$$v_m^* \to v_m^* + \Gamma^{-1} C_1 h^2 G' \quad (39)$$

where $\Delta v_m^* = \Gamma^{-1} C_1 h^2 G'$. In both cases, for realistic values of h and C_1, changes in interface velocity are proportional to the sign of G'. Substituting into ΔV gives:

$$\Delta V = v_m(t, G \to G + G') - v_m^*(t, G \to G + G') = G' \left(\frac{\kappa_i c_i}{L} - \Gamma^{-1} C_1 h^2 \right) \quad (40)$$

Taking generally representative values for the variables involved (Table 1) results in $\frac{\kappa_i c_i}{L} - \Gamma^{-1} C_1 h^2 < 0$ for all $h > 7.25 \times 10^{-4}$ m. The mushy layer thicknesses calculated in Sections 3.1-3.5 are greater than 1 mm thick for all ice shell thicknesses of interest. Thus,

$$\begin{cases} \Delta V < 0 & if \quad G' > 0 \\ \Delta V > 0 & if \quad G' < 0 \end{cases} \quad (41)$$

This suggests that if there is an increase in thermal gradient the mushy layer will thin, while if there is a decrease in thermal gradient the mushy layer will thicken. This is to be expected, as it was shown in Section 3.5 that equilibrium mushy layer thicknesses increased with decreasing thermal gradients. Figure 7 depicts the results of Section 3.5 along with the thickening/thinning trends induced by perturbations to the thermal gradient. The agreement between the two suggests that thermal gradient perturbations to a mushy layer originally in equilibrium (subject to the thermal gradient G) will lead to thickening/thinning of the mushy layer towards a new equilibrium mushy layer thickness governed by $G + G'$. This new equilibrium thickness will be greater than the original equilibrium thickness if $G' < 0$, and less than the original equilibrium thickness if $G' > 0$. The linear dependence of ΔV on G' ($\Delta V \propto G'$) means $\Delta V \to 0$ smoothly as $G' \to 0$, and, coupled with the linear and quadratic dependence of ΔV on h' ($\Delta V \propto h' + h'^2$), means that $\Delta V \to 0$ smoothly as the system moves towards its new equilibrium mushy layer thickness. Perturbations to thermal gradient alter the characteristic equilibrium state of the system, meaning the prior mushy layer thickness is no longer in equilibrium. The mushy layer responds by thickening/thinning until the new equilibrium state is reached.

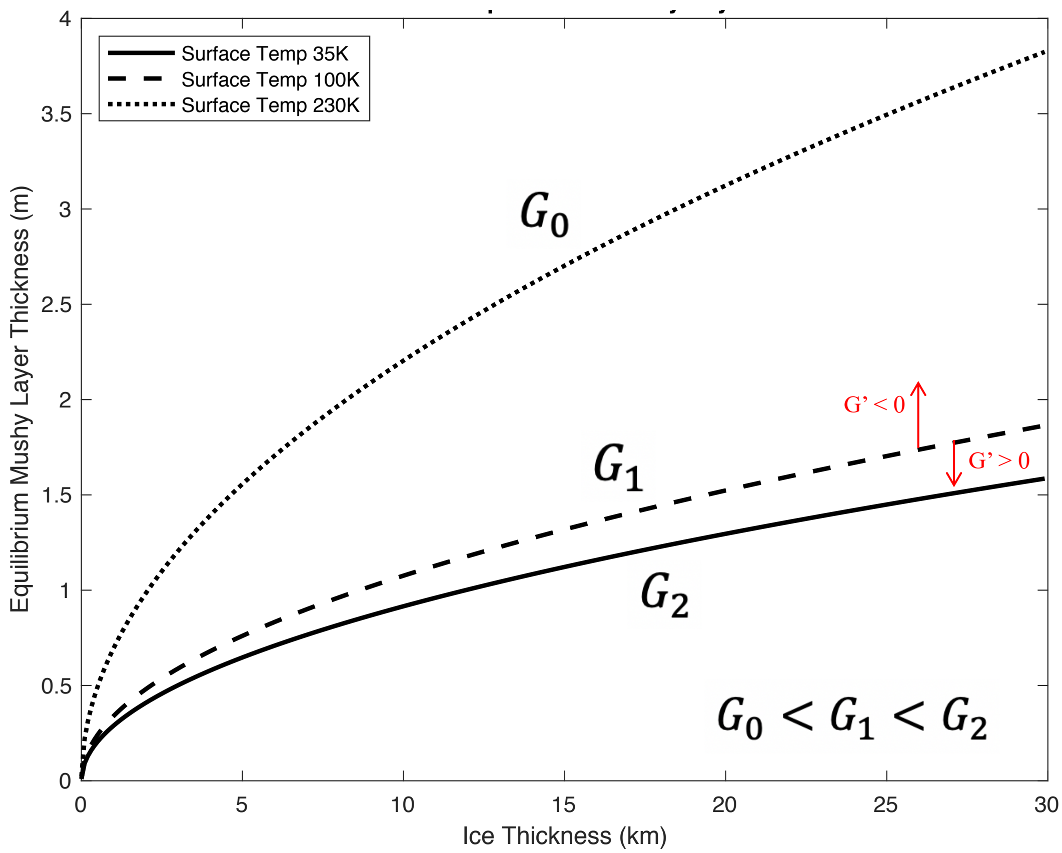

Figure 7 – Trends in equilibrium mushy layer thickness with thermal gradient perturbations. Shallower thermal gradients support thicker mushy layers than do steep thermal gradients (solid, dashed, and dotted black lines). Accordingly, perturbations which decrease/increase the thermal gradient tend to thicken/thin the mushy layer (red arrows and text).

Our sensitivity analysis of mushy layers subject to perturbations in physical (h) and environmental (T_S, T_{oc}, H) properties suggests they are likely a prevalent feature of ice-ocean worlds, persisting for long periods of time and characterizing the ice-ocean/brine interfaces of these systems. Thus, quantifying the multiphase physics that govern these boundary layers and their interactions with both the ocean and ice shell promises to drastically improve our understanding of ice-ocean world geophysical and biogeochemical processes.

4 Current Limitations

The use of reactive transport modeling to simulate ocean-derived ices is an active and ever evolving field spanning ocean, atmosphere, Earth systems, and planetary science. As such, it is instructive to assess the current limits of our knowledge on the subject and identify key outstanding questions as well as strategies to address them. Here, we highlight three of these limitations which are particularly important to the dynamics and evolution of planetary ice-ocean.

Two closely related problems are; 1) identifying if a critical porosity exists and if so, finding its value, and 2) constraining the permeability-porosity relationship of ocean-derived ices. Here, critical porosity is the liquid fraction at which fluid flow in the mushy layer ceases and is akin to a percolation threshold. In ice-ocean systems this is physically represented by the solidification of brine pockets and channels until their connectivity with the underlying ocean vanishes, leaving only isolated brine pockets which are incapable of brine drainage. Many models of sea ice implement a critical porosity of 5% [*Buffo et al.*, *2020; Buffo et al.*, 2018; *Wongpan et al.*, 2015]. While this estimate is broadly used by a number of successful models and is based on empirical observations [*Golden et al.*, 1998; *Golden et al.*, 2007], it remains a contentious subject in the community [*Hunke et al.*, 2011; *Turner and Hunke*, 2015; *Turner et al.*, 2013] and it has been shown that minimal variations in its value can appreciably affect estimates of sea ice bulk salinity [*Buffo et al.*, 2018]. In planetary applications some investigators implement a critical porosity [*Buffo et al.*, *2020; Hammond et al.*, 2018] while others allow fluid flow to persist for all non-zero porosities [*Hesse and Castillo-Rogez*, 2019; *Kalousová et al.*, 2014; 2016] suggesting brine can continue to percolate along grain boundaries. One consequence of excluding a critical porosity is the rapid downward transport of any water within an ice shell into the underlying ocean [*Hesse and Castillo-Rogez*, 2019; *Kalousová et al.*, 2014; 2016] which may not be reconcilable with geological and geophysical observations [*Schmidt et al.*, 2011]. While laboratory experiments have identified brine along grain boundaries in low temperature ices [*Desbois et al.*, 2008; *McCarthy et al.*, 2013], natural terrestrial ices are capable of supporting supraglacial and englacial hydrological systems [*Forster et al.*, 2014; *Koenig et al.*, 2014] suggesting a relative level of impermeability. Additionally, the surface of Europa exhibits numerous features which suggest that endogenic ocean material has been transported across the ice shell [*Kargel et al.*, 2000; *Zolotov and Shock*, 2001]. *Buffo* [2019] show that critical porosity likely plays a crucial role in determining the extent of impurity entrainment in planetary ices. The substantial effect of critical porosity on mushy layer equilibrium thickness can be seen in Figure 8, which solves Equation 25 for the equilibrium mushy layer thickness using three different critical porosities ($\phi_c = [0.01, 0.025, 0.05]$). Constraining the value of this parameter will improve estimates of ice shell composition and determine the rates of putative ocean-surface material transport.

A similar problem is determining the permeability of the mushy layer. This hurdle is common to all problems involving fluid transport in porous media [*Bear*, 2013]. The permeability is governed by the complex geometry and connectivity of the pore space, a difficult quantity to collect, especially for the fragile ice-ocean interface. Computed tomographic imagery of ice cores have begun to elucidate the complex temperature dependent evolution of brine pockets and channels in sea ice [*Golden et al.*, 2007]. In numerical models permeability is typically parameterized as a function of porosity (e.g. [*Griewank and Notz*, 2013; *Katz and Worster*, 2008; *Oertling and Watts*, 2004; *Wettlaufer et al.*, 2000]). While many of these parameterizations are capable of reproducing certain features of ice-ocean interface dynamics and evolution the choice of permeability-porosity relationship will affect the rate of impurity entrainment in the overlying ice and the structure of the mushy layer [*Buffo et al.*, *2020; Buffo et al.*, 2018]. For planetary applications, where observations of ice properties will be utilized to infer characteristics of subsurface water reservoirs and interior geophysical processes, constraining this relationship is of the utmost importance. In analogy to terrestrial ice biogeochemistry this could have profound impacts on nutrient availability and substrate evolution in a boundary layer that could be quite favorable for life [*Loose et al.*, 2011; *Thomas and Dieckmann*, 2003]. Moreover, the permeability and meltwater content of ice streams on Earth strongly affect their rheology and large-scale dynamics [*Haseloff et al.*, 2019; *Meyer and Minchew*, 2018], suggesting these properties may have substantial implications for the global geodynamics of planetary ice shells as well (e.g. solid-state convection).

Finally, planetary ice-ocean environments are likely subject to thermal, chemical, and physical regimes that are substantially different than those found on Earth. Laboratory experiments have demonstrated that, upon freezing, brines of different compositions produce ices with diverse microstructural properties [*McCarthy et al.*, 2007]. These small-scale structural differences may result in drastically different thermodynamic, mechanical, and fluid transport properties, suggesting that ice-ocean worlds of different compositions may exhibit unique ice shell dynamics. In Section 3.1-3.5 it was shown that variable physical and thermochemical pressures effect the geometry of the ice-ocean interface mushy layer, which may impact energy and material transport rates between the ocean and overlying ice shell. Continued theoretical and laboratory investigations promise to improve our understanding of planetary ice properties and will inform both numerical models and the analysis of future spacecraft observations (e.g. Europa Clipper's ice penetrating radar, REASON, which critically depends on the dielectric properties and heterogeneity of the ice shell [*Di Paolo et al.*, 2016; *Grima et al.*, 2016; *Kalousova et al.*, 2017; *Moore*, 2000]).

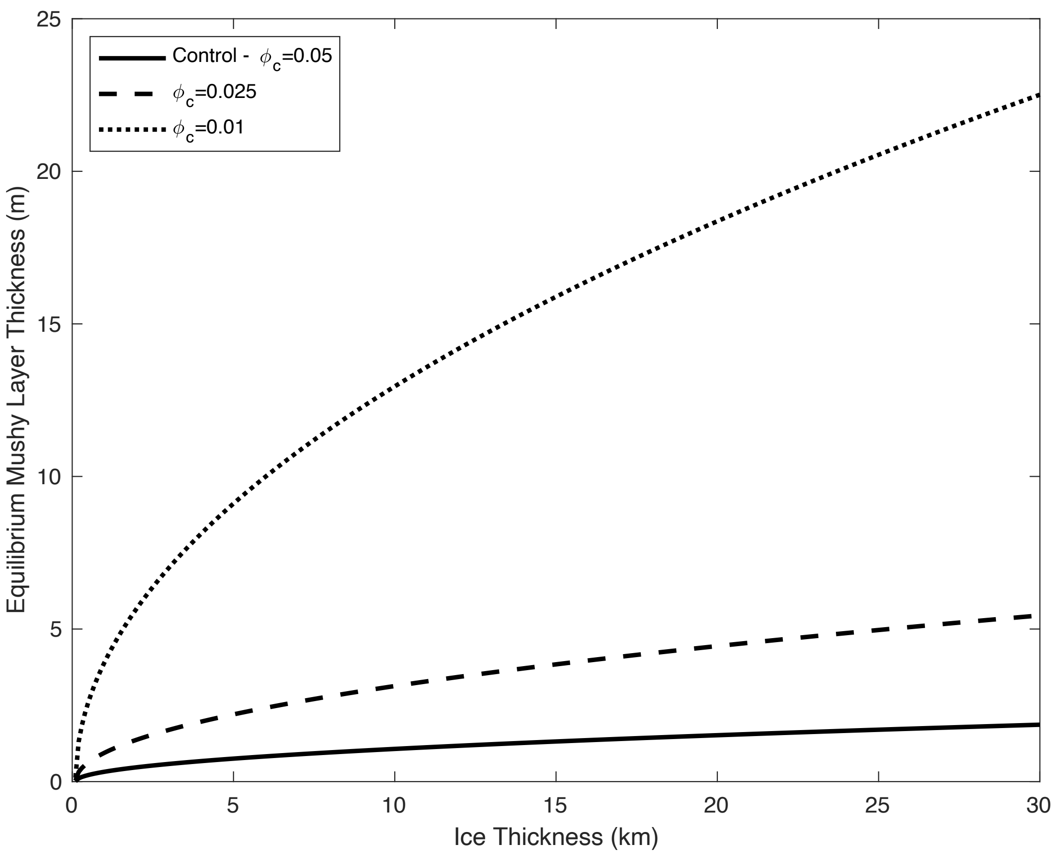

Figure 8 – The effect of critical porosity on equilibrium mushy layer thickness. Reducing the critical porosity leads to substantially thicker mushy layers as brine flow is greatly restricted at low porosities.

5 Discussion

5.1 Mushy Layers on Ice-Ocean Worlds

We have shown that a variety of realistic environmental pressures likely supports a diverse population of stable ice-ocean mushy layers spread across the icy worlds of our solar system. The ubiquity of ice-ocean worlds and their prominence amongst high priority astrobiology targets has led to a substantial interest in understanding and constraining their geophysical and biogeochemical dynamics and evolution [*Council*, 2012; *Des Marais et al.*, 2008]. The ice-ocean interface has been repeatedly identified as an important control on ice shell and ocean processes [*Allu Peddinti and McNamara*, 2015; *Barr and McKinnon*, 2007; *Buffo et al.*, *2020; Buffo et al.*, 2019; *Schmidt et al.*, 2017; *Soderlund et al.*, 2014], yet its properties remain largely unconstrained, and it is frequently treated as a chemically inert and abrupt ice-liquid phase boundary. Exclusion of the multiphase mushy layer prevents accurate simulation of the interface's thermal and physicochemical dynamics, which will directly impact; thermocompositional convection in the ice shell [*Pappalardo and Barr*, 2004], ocean-surface material transport [*Allu Peddinti and McNamara*, 2015], the entrainment, transport, and potential expression of ocean-derived biosignatures [*Schmidt*, 2020; *Schmidt et al.*, 2017], ice shell mechanical, eutectic, and dielectric properties [*Durham et al.*, 2005; *Kalousova et al.*, 2017; *McCarthy et al.*, 2011; *Toner et al.*, 2014], and intrashell hydrology [*Schmidt et al.*, 2011]. While our results suggest the ice-ocean mushy layer is geophysically thin (~1-30 m), it acts as a mandatory port of call for any and all ice-ocean-surface exchange on icy worlds, making it a crucial boundary from both a geophysical and astrobiological perspective as it will govern the biogeochemistry of the overlying ice shell. Additionally, our selection of a critical porosity of 5% means our mushy layer thickness predictions are for the active two-phase regions of ice shell where hydraulic conductivity to the underlying ocean is present. The extent of the region where disconnected brine pockets are stable could likely extend much further into the ice shell (e.g. eutectic horizons [*Vance et al.*, 2019; *Zolotov et al.*, 2004]), however the properties of this region will also be governed by the mushy layer environment in which it originally formed. Our results provide an efficient method to quantify the characteristics of this important layer for any ice-ocean/brine system. The broad applicability of this technique and its analytical nature means that it can be easily implemented and utilized in any investigation seeking to include the first order effects of treating the ice-ocean interface as a multiphase mushy layer. With stark similarities between the ice-ocean systems of icy worlds and magmatic systems on Earth and the immense impact of reactive transport modeling on our understanding of geoscience, including such physics could undoubtedly enhance our understanding of ice-ocean systems.

5.2 Heterogeneities and Depositional Processes Within Growing Mushy Layers

5.2.1 Fluid Flow and Brine Channel Formation

Mushy layers themselves are inhomogeneous and support an array of structural, thermal, and compositional heterogeneities [*Buffo et al.*, 2018; *Golden et al.*, 2007; *Wells et al.*, 2011; *Wettlaufer et al.*, 1997a; b; *Worster et al.*, 1990; *Worster and Rees Jones*, 2015]. The complexity and small scale of these heterogenous features leads to their frequent exclusion from numerical models (e.g. [*Bitz and Lipscomb*, 1999; *Griewank and Notz*, 2015; *Hunke et al.*, 2011]). An archetype example of mushy layer heterogeneity is the formation and dynamics of brine channels. A byproduct of the convective downwelling of concentrated interstitial pore fluid, these dendritic channel structures play a fundamental role in the thermal and physicochemical evolution of the mushy layer [*Griewank and Notz*, 2013; *Rees Jones and Worster*, 2013; *Turner et al.*, 2013; *Wells et al.*, 2010; 2011]. Nearly all models of ice-ocean interface dynamics and evolution are one-dimensional, necessitating parameterization of the inherently two-dimensional process of brine channel formation and evolution. Frequently the convective flow through these channels is parameterized using optimization arguments, and a number of successful parameterizations exist [*Buffo et al.*, 2018; *Griewank and Notz*, 2013; *Hunke et al.*, 2011; *Turner and Hunke*, 2015; *Turner et al.*, 2013; *Wells et al.*, 2010; 2011]. However, these parameterizations employ isotropy and homogeneity (e.g. brine channel spacing, mushy layer permeabilities) that may not be representative of a dynamic natural system. In both laboratory and natural environments heterogenous brine channel and brinicle formation and evolution are observed [*Golden et al.*, 2007; *Notz and Worster*, 2008; *Wettlaufer et al.*, 1997b; *Worster and Rees Jones*, 2015]. Such heterogeneities may induce lateral variation in mushy layer physicochemical and transport properties. Constraining the interdependence of environmental parameters and mushy layer heterogeneity is imperative in understanding the dynamics and evolution of these active interfaces. In magmatic systems it is these small-scale heterogeneous drainage processes that determine the structure and composition of the resultant rock [*Fowler*, 1987; *Jordan and Hesse*, 2015; *Reiners*, 1998; *Worster et al.*, 1990].

Contemporary models have begun to simulate mushy layer formation in two dimensions, removing the need for parameterization of pore fluid convection [*Katz and Worster*, 2008; *Oertling and Watts*, 2004; *Wells et al.*, 2019]. These models successfully simulate the onset of density instabilities and convection in the mushy layer, leading to the formation and evolution of brine channels. While the spatiotemporal extent of these models is limited by the substantial computational cost of simulating such detailed multiphase reactive transport processes, they provide an unparalleled method for understanding the role of heterogeneities in the dynamics and evolution of mushy layers as well as a numerical technique that can be extended to include additional physics or tailored to simulate diverse ice-ocean environments. Recently, *Parkinson et al.* [2020] combined a two-dimensional reactive transport model with the method of adaptive mesh refinement to efficiently simulate the solidification of binary alloys, such as ice-ocean/brine systems. They showed that such a technique can drastically reduce the computation time of such simulations while still resolving the fine-scale structure of convection and brine channel formation in the mushy layer. Such an approach could be extremely beneficial in simulating the two-phase dynamics and evolution of planetary ice shells as they likely contain processes which occur over a wide range of spatial and temporal scales.

5.2.2 Ice Diagenesis

Ice-ocean interfaces may be additionally modified by depositional processes, wherein ice crystals nucleated in the underlying water column buoyantly sediment onto the basal ice interface. This process has been observed under ice shelves and ice shelf adjacent sea ice in Antarctica where the accretion of frazil and platelet ice leads to the formation of porous marine ice and sub-ice platelet layers beneath ice shelves and sea ice, respectively [*Buffo et al.*, 2018; *Craven et al.*, 2009; *Dempsey et al.*, 2010; *Fricker et al.*, 2001; *Langhorne et al.*, 2015; *Robinson et al.*, 2014]. On Earth, these depositional processes are driven by the ice pump mechanism, where ice shelf basal melting and topography drives the formation of buoyant supercooled water plumes – the source of both frazil and platelet ice [*Lewis and Perkin*, 1983]. Similar depositional processes have been theorized to occur on other ice-ocean worlds, potentially driven by ocean currents and/or latitudinal variations in basal ice topography [*Soderlund et al.*, 2014]. The buoyancy driven sedimentation of ice crystals onto the ice-ocean interface will further modify the mushy layer. No longer driven solely by thermodynamic heat loss to the overlying ice, a high porosity layer of deposited crystals begins to form if the advancing ice-mush interface velocity does not match that of the sedimentation rate [*Buffo et al.*, 2018]. In these accreted regions porosity is dependent on the packing efficiency and ensuing buoyancy driven compaction of the deposited ice crystals. Unconsolidated platelet ice layers beneath ice shelf adjacent sea ice can have porosities as high as 25% [*Gough et al.*, 2012; *Wongpan et al.*, 2015] and sub-ice shelf marine ice can remain hydraulically connected to the underlying ocean as far as ~70 m above the ice-ocean interface [*Craven et al.*, 2009]. Under such conditions, the combined depositional, thermal, chemical, and mechanical processes occurring in the layer will govern the evolution of the ice-ocean interface.

An analogous process of deposition, compaction, and thermochemical evolution governs the diagenesis of marine sediments [*Berner*, 1980]. Providing a gradient rich medium for benthic fauna in terrestrial oceans, the ice-ocean interface of worlds like Europa may supply an analogous inverted substrate for potential organisms. This possibility is strengthened by the likelihood that these interfaces exist as persistently multiphase boundaries, akin to those that support substantial biological communities at the base of sea ice and ice shelves on Earth [*Daly et al.*, 2013; *Krembs et al.*, 2011; *Loose et al.*, 2011; *Vancoppenolle et al.*, 2013]. The formation of brinicles on Europa has been suggested as a process which could produce chemical gradients similar to those observed in chemical gardens and hydrothermal regions of the terrestrial ocean, oases for benthic ecology [*Vance et al.*, 2019]. Additionally, in the case of Europa, it has been suggested that delivery of surface derived oxidants to a reduced ocean may drive redox potentials favorable to the reactions of metabolic processes [*Chyba and Phillips*, 2001; *Hand et al.*, 2007; *Vance et al.*, 2016; *Vance et al.*, 2018]. As the boundary where these oxidants would be introduced into the ocean, the ice-ocean interface could provide a chemical boon for any prospective biosphere in an otherwise potentially oligotrophic water column. In turn, akin to both terrestrial sea ice communities [*Krembs et al.*, 2011] and bioturbation in marine sediments [*Berner*, 1980], any potential biosphere will likely alter the evolution of the host ice-ocean substrate. Understanding how organisms interact with and depend upon the microstructural and chemical evolution of ice-ocean interfaces will help constrain the habitability of these environments and the role biogeochemical processes play in the dynamics of these active boundary layers. Furthermore, quantifying the entrainment of biosignatures within forming ices will aid in predicting the likelihood of ocean-surface transport and surface expression of ocean-derived materials on icy worlds.

While no models of two-dimensional reactive transport or biosignature entrainment currently exist for planetary ices, a number of one-dimensional reactive transport and compaction models [*Buffo et al.*, *2020; Hammond et al.*, 2018] and two-dimensional multiphase models [*Hesse and Castillo-Rogez*, 2019; *Kalousová et al.*, 2014; 2016] have been used to investigate the thermochemical evolution and dynamics of ice-ocean worlds. These existing models can be leveraged alongside contemporary models of sea ice, which include formalisms for simulating small-scale heterogeneities within the mushy layer [*Katz and Worster*, 2008; *Oertling and Watts*, 2004; *Parkinson et al.*, 2020; *Wells et al.*, 2019] and biogeochemical processes [*Tedesco and Vichi*, 2014; *Vancoppenolle et al.*, 2013; *Vancoppenolle and Tedesco*, 2015], to improve our understanding of the role ice-ocean interfaces play in governing the geophysics and habitability of ice-ocean worlds.

5.3 Vanishing Mushy Layers in Equilibrated Ice Shells

Planetary ice shells are dynamic and complex systems whose evolutions are governed by much more than conductive heat loss and solute transport near the ice-ocean interface. The analytic results presented above provide a powerful tool to estimate the properties and dynamics of a diverse array of ice-ocean/brine interfaces, however these results have focused on ice shells that are still thickening. While this is certainly an important stage in the evolution of an ice shell, it is possible that these ice shells reach a quasi-equilibrium thickness – undergoing oscillatory thinning and thickening [*Hussmann and Spohn*, 2004; *Hussmann et al.*, 2002]. In many cases, take for example Europa, this equilibrium thickness is facilitated by the dissipation of tidal energy into the ice shell, effectively warming the shell to a point where the moon's total outward heat flux has reached a steady state [*Hussmann et al.*, 2002]. In this scenario, propagation of the mush-ocean interface would cease ($\dot{z}_m(t) \to 0$). The ice-mush interface ($z_m^*(t)$), however, would still be in chemical disequilibrium with the underlying ocean and would continue to propagate until it reached the stagnated mush-ocean interface. This phenomenon has been predicted theoretically and observed in laboratory grown mushy layers [*Gewecke and Schulze*, 2011a; b; *Huguet et al.*, 2016] and at the ice-ocean interface of thinning sea ice [*Petrich and Eicken*, 2010]. This suggests that ice shells in thermal equilibrium could lose their ice-ocean interface mushy layers during periods of stagnated growth or thinning, instead possessing a more abrupt solid-liquid transition, void of any two-phase region, which would impact thermal and chemical transport between the ice shell and ocean as well as the interface's astrobiological potential. The elimination of a mushy layer would leave conduction as the sole mechanism of heat transport between the ice shell and ocean. Solute rejection would likely become extremely efficient, no longer trapping brine in the pores and channels of a two-phase boundary, suggesting impurity entrainment limits governed by partition coefficients [*Weeks and Lofgren*, 1967; *Wolfenbarger et al.*, 2019] rather than critical porosity/percolation thresholds [*Buffo et al., 2020; Golden et al.*, 1998; *Golden et al.*, 2007]. Furthermore, the porous substrate which provides a habitat for ice-dwelling organisms in terrestrial analog ices [*Loose et al.*, 2011; *Thomas and Dieckmann*, 2003; *Wettlaufer*, 2010] could be lost.

It is important to note that this does not preclude the existence of contemporary ice-ocean interface mushy layers on icy worlds within the solar system. Cyclic thickening could be driven by orbital evolution [*Hussmann and Spohn*, 2004; *Hussmann et al.*, 2002] and regional redistribution and growth of ice could be driven by interior processes such as ocean circulation [*Soderlund et al.*, 2014; *Soderlund*, 2019]. Furthermore, fractures at the base of the ice shell would be rapidly infilled or refrozen by new ice, similar to basal fractures and rifts in terrestrial ice shelves [*Khazendar and Jenkins*, 2003; *Khazendar et al.*, 2009], facilitating the formation of localized mushy layers and entraining ocean derived material in these features [*Buffo et al.*, *2020*]. On icy worlds such features could promote ocean-surface material transport and present as extensional terrain [*Howell and Pappalardo*, 2018], facilitate hydrological processes in the shell through diking [*Craft et al.*, 2016; *Manga and Michaut*, 2017; *Michaut and Manga*, 2014], or be the source of plumes [*Brown et al.*, 1990; *Fagents et al.*, 2000; *Glein and Shock*, 2010; *Hansen et al.*, 2011; *Sparks et al.*, 2016]. With their relation to geophysically active regions on ice-ocean worlds, understanding the properties and evolution of these features is of substantial value. The technique we outline here can be easily adapted to the geometries and thermal environments of these systems to investigate their interfacial dynamics.

6 Conclusion

Our work demonstrates that the transition between solid ice and ocean in icy worlds is likely much more dynamic than has been accounted for in most models. By appealing to the importance mushy layers play in terrestrial analog systems, namely the thermochemical and biological impacts of the two-phase ice-ocean interface of sea ice, and the geophysical implications of mushy layers in magmatic systems, we derive approximations that define the regimes where these physics become important to how we observe and interpret planetary data. Solving for the equilibrium mushy layer thickness of the simplified ice-mush-ocean system presented in Section 2 allows us to investigate the impacts various environmental parameters have on mushy layer properties. In so doing, we begin to constrain the characteristics, dynamics, and evolution of ice-ocean interfaces across different icy worlds. Lower gravity bodies support thicker mushy layers, suggesting that the inner ice shell of a small moon like Enceladus may remain much more hydraulically connected to the underlying ocean than the deep ice shell of a larger body (e.g. Europa). For Enceladus this will impact the dynamics of basally driven geophysical and transport processes within the ice shell, such as fracture formation and evolution as well as plume generation and dynamics. Identifying whether plumes could be sourced from concentrated or highly processed pore fluid within the shell has the potential to drastically alter our interpretation of spacecraft data. Moreover, because mushy layer thickness is inversely related to thermal gradient, as ice shells thicken so do their interfacial mushy layers, making reactive transport processes at or near the ice-ocean interface more important as the ice grows. Ocean composition has a substantial effect on mushy layer properties, suggesting that variations in liquid chemistries between bodies, or within the same body, may result in different mushy layer characteristics. All of these results also depend critically on permeability and porosity; which have a drastic effect on mushy layer geometry and dynamics. We emphasize that these elusive parameters (porosity, permeability, and the relation between them) play a crucial role in the physics governing the dynamics and evolution of ice shells and mushy layers and that future work quantifying their values in ice-ocean systems will drastically improve ice-ocean world models. Regardless, mushy layers are stable structures in thickening ice shells that maintain nonzero equilibrium thicknesses when subject to perturbations in thickness and thermal gradient, suggesting mushy layers are likely common and persistent features of accretionary ice-ocean interfaces throughout the solar system.

As a dynamic physical and thermochemical boundary, the ice-ocean interface of ocean worlds likely plays a crucial role in their geophysics and habitability. Persisting as geophysically thin porous layers governed by multiphase reactive transport processes they dictate the thermochemical evolution of the overlying ice and may provide a gradient rich oasis for potential astrobiology. A number of terrestrial analogs provide invaluable resources when designing and validating models seeking to simulate planetary ice-ocean systems. With mounting evidence supporting the notion that ice shells are heterogeneous and active structures that may harbor ongoing hydrological processes constraining the effects of multiphase dynamics on their evolution is an imperative progression in simulating ice-ocean world geophysics and biogeochemical cycling. Our results, which constitutes a broadly applicable method for characterizing ice-ocean/brine interfaces, can be used to provide refined boundary conditions for both ocean and ice shell models in the form of improved thermochemical flux estimates and boundary layer properties (e.g. two-phase layer thickness, ice-ocean hydraulic connectivity). Additionally, this technique could be implemented to supply testable predictions about the structure and properties of planetary ice shells, insofar as identifying thermal, physicochemical, and dielectric signatures of multiphase layers which could be observed by upcoming missions (in particular, ice penetrating radar measurements).The inclusion of reactive transport processes in models of terrestrial geophysics has revolutionized our understanding of the Earth system. With enhanced spacecraft observations and advances in computing power, a comparable renaissance in the field of ice-ocean worlds may be afoot.

References

Aagaard, K., and E. C. Carmack (1989), The Role of Sea Ice and Other Fresh-Water in the Arctic Circulation, *Journal of Geophysical Research-Oceans*, *94*(C10), 14485-14498, doi:DOI 10.1029/JC094iC10p14485.

Allu Peddinti, D., and A. K. McNamara (2015), Material transport across Europa's ice shell, *Geophysical Research Letters*, *42*(11), 4288-4293, doi:10.1002/2015GL063950.

Balmforth, N. J., J. S. Wettlaufer, and G. Worster (2007), 2006 Program of Study: Ice*Rep.*, WOODS HOLE OCEANOGRAPHIC INSTITUTION MA DEPT OF PHYSICAL OCEANOGRAPHY.

Barr, A. C., and W. B. McKinnon (2007), Convection in ice I shells and mantles with self-consistent grain size, *Journal of Geophysical Research: Planets*, *112*(E2), doi:10.1029/2006JE002781.

Bear, J. (2013), *Dynamics of fluids in porous media*, Courier Corporation.

Berner, R. A. (1980), *Early diagenesis: a theoretical approach*, Princeton University Press.

Bitz, C. M., and W. H. Lipscomb (1999), An energy-conserving thermodynamic model of sea ice, *Journal of Geophysical Research: Oceans*, *104*(C7), 15669-15677.

Braun, J. (2010), The many surface expressions of mantle dynamics, *Nature Geoscience*, *3*(12), 825-833, doi:10.1038/Ngeo1020.

Brown, R. H., R. L. Kirk, T. V. Johnson, and L. A. Soderblom (1990), Energy Sources for Triton's Geyser-Like Plumes, *Science*, *250*(4979), 431-435, doi:10.1126/science.250.4979.431.

Buffo, J., B. Schmidt, C. Huber, and C. Walker (*2020*), Entrainment and dynamics of ocean-derived impurities within Europa's ice shell, *JGR: Planets*.

Buffo, J., B. Schmidt, A. Pontefract, and J. Lawrence (2019), Frozen Fingerprints: Chemical and Biological Entrainment in Planetary Ices, in *Astrobiology Science Conference*, edited, Bellevue, Washington.

Buffo, J. J. (2019), Multiphase reactive transport in planetary ices, Georgia Institute of Technology.

Buffo, J. J., B. E. Schmidt, and C. Huber (2018), Multiphase Reactive Transport and Platelet Ice Accretion in the Sea Ice of McMurdo Sound, Antarctica, *Journal of Geophysical Research-Oceans*, *123*(1), 324-345, doi:10.1002/2017jc013345.

Burke, K., B. Steinberger, T. H. Torsvik, and M. A. Smethurst (2008), Plume generation zones at the margins of large low shear velocity provinces on the core-mantle boundary, *Earth and Planetary Science Letters*, *265*(1-2), 49-60, doi:10.1016/j.epsl.2007.09.042.

Čadek, O., G. Tobie, T. Van Hoolst, M. Massé, G. Choblet, A. Lefèvre, G. Mitri, R. M. Baland, M. Běhounková, and O. Bourgeois (2016), Enceladus's internal ocean and ice shell constrained from Cassini gravity, shape, and libration data, *Geophysical Research Letters*, *43*(11), 5653-5660.

Carr, M. H. (1987), Water on Mars, *Nature*, *326*(6108), 30-35, doi:DOI 10.1038/326030a0.

Carr, M. H., et al. (1998), Evidence for a subsurface ocean on Europa, *Nature*, *391*(6665), 363-365, doi:10.1038/34857.

Castillo-Rogez, J. C., and T. B. McCord (2010), Ceres' evolution and present state constrained by shape data, *Icarus*, *205*(2), 443-459, doi:10.1016/j.icarus.2009.04.008.

Chyba, C., and C. Phillips (2001), Possible ecosystems and the search for life on Europa, *Proc Natl Acad Sci U S A*, *98*(3), 801-804, doi:10.1073/pnas.98.3.801.

Cottier, F., H. Eicken, and P. Wadhams (1999), Linkages between salinity and brine channel distribution in young sea ice, *Journal of Geophysical Research-Oceans*, *104*(C7), 15859-15871, doi:Doi 10.1029/1999jc900128.

Council, N. R. (2012), *Vision and voyages for planetary science in the decade 2013-2022*, National Academies Press.

Cox, G. F., and W. F. Weeks (1974), Salinity variations in sea ice, *Journal of Glaciology*, *13*(67), 109-120.

Craft, K. L., G. W. Patterson, R. P. Lowell, and L. Germanovich (2016), Fracturing and flow: Investigations on the formation of shallow water sills on Europa, *Icarus*, *274*, 297-313, doi:10.1016/j.icarus.2016.01.023.

Craven, M., I. Allison, H. A. Fricker, and R. Warner (2009), Properties of a marine ice layer under the Amery Ice Shelf, East Antarctica, *Journal of Glaciology*, *55*(192), 717-728, doi:Doi 10.3189/002214309789470941.

Daly, M., F. Rack, and R. Zook (2013), Edwardsiella andrillae, a new species of sea anemone from Antarctic ice, *PLoS One*, *8*(12), e83476, doi:10.1371/journal.pone.0083476.

De Sanctis, M., A. Raponi, E. Ammannito, M. Ciarniello, M. Toplis, H. McSween, J. Castillo-Rogez, B. Ehlmann, F. Carrozzo, and S. Marchi (2016), Bright carbonate deposits as evidence of aqueous alteration on (1) Ceres, *Nature*, *536*(7614), 54.

Dempsey, D. E., P. J. Langhorne, N. J. Robinson, M. J. M. Williams, T. G. Haskell, and R. D. Frew (2010), Observation and modeling of platelet ice fabric in McMurdo Sound, Antarctica, *Journal of Geophysical Research-Oceans*, *115*(C1), doi:Artn C0100710.1029/2008jc005264.

Des Marais, D. J., et al. (2008), The NASA Astrobiology Roadmap, *Astrobiology*, *8*(4), 715-730, doi:10.1089/ast.2008.0819.

Desbois, G., J. Urai, C. Burkhardt, M. Drury, M. Hayles, and B. Humbel (2008), Cryogenic vitrification and 3D serial sectioning using high resolution cryo-FIB SEM technology for brine-filled grain boundaries in halite: first results, *Geofluids*, *8*(1), 60-72.

Di Paolo, F., S. E. Lauro, D. Castelletti, G. Mitri, F. Bovolo, B. Cosciotti, E. Mattei, R. Orosei, C. Notarnicola, and L. Bruzzone (2016), Radar signal penetration and horizons detection on Europa through numerical simulations, *IEEE Journal of Selected Topics in Applied Earth Observations and Remote Sensing*, *10*(1), 118-129.

Dickson, R. R., and J. Brown (1994), The Production of North-Atlantic Deep-Water - Sources, Rates, and Pathways, *Journal of Geophysical Research-Oceans*, *99*(C6), 12319-12341, doi:Doi 10.1029/94jc00530.

Durham, W. B., L. A. Stern, T. Kubo, and S. H. Kirby (2005), Flow strength of highly hydrated Mg-and Na-sulfate hydrate salts, pure and in mixtures with water ice, with application to Europa, *Journal of Geophysical Research: Planets*, *110*(E12).

Eicken, H. (1992), Salinity Profiles of Antarctic Sea Ice - Field Data and Model Results, *Journal of Geophysical Research-Oceans*, *97*(C10), 15545-15557, doi:Doi 10.1029/92jc01588.

Eicken, H., H. R. Krouse, D. Kadko, and D. K. Perovich (2002), Tracer studies of pathways and rates of meltwater transport through Arctic summer sea ice, *Journal of Geophysical Research-Oceans*, *107*(C10), SHE 22-21-SHE 22-20, doi:Artn 8046 10.1029/2000jc000583.

Fagents, S. A. (2003), Considerations for effusive cryovolcanism on Europa: The post-Galileo perspective, *Journal of Geophysical Research: Planets*, *108*(E12).

Fagents, S. A., R. Greeley, R. J. Sullivan, R. T. Pappalardo, L. M. Prockter, and G. S. Team (2000), Cryomagmatic mechanisms for the formation of Rhadamanthys linea, triple band margins, and other low-albedo features on Europa, *Icarus*, *144*(1), 54-88, doi:DOI 10.1006/icar.1999.6254.

Fanale, F. P., J. C. Granahan, T. B. McCord, G. Hansen, C. A. Hibbitts, R. Carlson, D. Matson, A. Ocampo, L. Kamp, and W. Smythe (1999), Galileo's multiinstrument spectral view of Europa's surface composition, *Icarus*, *139*(2), 179-188.

Feltham, D. L., N. Untersteiner, J. S. Wettlaufer, and M. G. Worster (2006), Sea ice is a mushy layer, *Geophysical Research Letters*, *33*(14), doi:Artn L14501 10.1029/2006gl026290.

Foley, B. J., and T. W. Becker (2009), Generation of plate-like behavior and mantle heterogeneity from a spherical, viscoplastic convection model, *Geochemistry, Geophysics, Geosystems*, *10*(8).

Forster, R. R., et al. (2014), Extensive liquid meltwater storage in firn within the Greenland ice sheet, *Nature Geoscience*, *7*(2), 95-98, doi:10.1038/Ngeo2043.

Fortes, A. D. (2000), Exobiological implications of a possible ammonia-water ocean inside Titan, *Icarus*, *146*(2), 444-452, doi:DOI 10.1006/icar.2000.6400.

Fowler, A. (1987), Theories of mushy zones: applications to alloy solidification, magma transport, frost heave and igneous intrusions, in *Structure and Dynamics of Partially Solidified Systems*, edited, pp. 159-199, Springer.

Freitag, J. (1999), The hydraulic properties of Arctic sea ice-Implications for the small-scale particle transport, *Ber. Polarforsch*, *325*, 150.

Fricker, H. A., S. Popov, I. Allison, and N. Young (2001), Distribution of marine ice beneath the Amery Ice Shelf, *Geophysical Research Letters*, *28*(11), 2241-2244, doi:Doi 10.1029/2000gl012461.

Gaeman, J., S. Hier-Majumder, and J. H. Roberts (2012), Sustainability of a subsurface ocean within Triton's interior, *Icarus*, *220*(2), 339-347, doi:10.1016/j.icarus.2012.05.006.

Gewecke, N. R., and T. P. Schulze (2011a), The rapid advance and slow retreat of a mushy zone, *Journal of Fluid Mechanics*, *674*, 227-243, doi:10.1017/S0022112011000103.

Gewecke, N. R., and T. P. Schulze (2011b), Solid-mush interface conditions for mushy layers, *Journal of Fluid Mechanics*, *689*, 357-375, doi:10.1017/jfm.2011.420.

Glein, C. R., and E. L. Shock (2010), Sodium chloride as a geophysical probe of a subsurface ocean on Enceladus, *Geophysical Research Letters*, *37*(9), doi:Artn L09204 10.1029/2010gl042446.

Golden, K. M., S. F. Ackley, and V. V. Lytle (1998), The percolation phase transition in sea Ice, *Science*, *282*(5397), 2238-2241, doi:10.1126/science.282.5397.2238.

Golden, K. M., H. Eicken, A. L. Heaton, J. Miner, D. J. Pringle, and J. Zhu (2007), Thermal evolution of permeability and microstructure in sea ice, *Geophysical Research Letters*, *34*(16), doi:Artn L16501 10.1029/2007gl030447.

Goodman, J. C., and E. Lenferink (2012), Numerical simulations of marine hydrothermal plumes for Europa and other icy worlds, *Icarus*, *221*(2), 970-983, doi:10.1016/j.icarus.2012.08.027.

Gough, A. J., A. R. Mahoney, P. J. Langhorne, M. J. M. Williams, N. J. Robinson, and T. G. Haskell (2012), Signatures of supercooling: McMurdo Sound platelet ice, *Journal of Glaciology*, *58*(207), 38-50, doi:10.3189/2012JoG10J218.

Greeley, R., C. F. Chyba, J. Head, T. McCord, W. B. McKinnon, R. T. Pappalardo, and P. H. Figueredo (2004), Geology of Europa, *Jupiter: The Planet, Satellites and Magnetosphere*, 329-362.

Griewank, P. J., and D. Notz (2013), Insights into brine dynamics and sea ice desalination from a 1-D model study of gravity drainage, *Journal of Geophysical Research: Oceans*, *118*(7), 3370-3386.

Griewank, P. J., and D. Notz (2015), A 1-D modelling study of Arctic sea-ice salinity, *Cryosphere*, *9*(1), 305-329, doi:10.5194/tc-9-305-2015.

Grima, C., J. S. Greenbaum, E. J. L. Garcia, K. M. Soderlund, A. Rosales, D. D. Blankenship, and D. A. Young (2016), Radar detection of the brine extent at McMurdo Ice Shelf, Antarctica, and its control by snow accumulation, *Geophysical Research Letters*, *43*(13), 7011-7018, doi:10.1002/2016gl069524.

Grumbine, R. W. (1991), A model of the formation of high-salinity shelf water on polar continental shelves, *Journal of Geophysical Research: Oceans*, *96*(C12), 22049-22062.

Hammond, N. P., E. Parmenteir, and A. C. Barr (2018), Compaction and Melt Transport in Ammonia-Rich Ice Shells: Implications for the Evolution of Triton, *Journal of Geophysical Research: Planets*, *123*(12), 3105-3118.

Hand, K. P., R. W. Carlson, and C. F. Chyba (2007), Energy, chemical disequilibrium, and geological constraints on Europa, *Astrobiology*, *7*(6), 1006-1022, doi:10.1089/ast.2007.0156.

Hansen, C. J., et al. (2011), The composition and structure of the Enceladus plume, *Geophysical Research Letters*, *38*(11), doi:Artn L11202 10.1029/2011gl047415.

Haseloff, M., I. J. Hewitt, and R. F. Katz (2019), Englacial Pore Water Localizes Shear in Temperate Ice Stream Margins, *Journal of Geophysical Research-Earth Surface*, *124*(11), 2521-2541, doi:10.1029/2019jf005399.

Head, J., R. Pappalardo, R. Greeley, R. Sullivan, C. Pilcher, G. Schubert, W. Moore, M. Carr, J. Moore, and M. Belton (1997), Evidence for recent solid-state convection on Europa: The nature of pits, domes, spots, and ridges, paper presented at Bulletin of the American Astronomical Society.

Head, J. W., R. T. Pappalardo, and R. Sullivan (1999), Europa: Morphological characteristics of ridges and triple bands from Galileo data (E4 and E6) and assessment of a linear diapirism model, *Journal of Geophysical Research-Planets*, *104*(E10), 24223-24236, doi:Doi 10.1029/1998je001011.

Hesse, M., and J. Castillo-Rogez (2019), Thermal Evolution of the Impact-Induced Cryomagma Chamber Beneath Occator Crater on Ceres, *Geophysical Research Letters*, *46*(3), 1213-1221.

Howell, S. M., and R. T. Pappalardo (2018), Band formation and ocean-surface interaction on Europa and Ganymede, *Geophysical Research Letters*, *45*(10), 4701-4709.

Howell, S. M., and R. T. Pappalardo (2019), Can Earth-like plate tectonics occur in ocean world ice shells?, *Icarus*, *322*, 69-79.

Huber, C., O. Bachmann, and M. Manga (2009), Homogenization processes in silicic magma chambers by stirring and mushification (latent heat buffering), *Earth and Planetary Science Letters*, *283*(1-4), 38-47, doi:10.1016/j.epsl.2009.03.029.

Huber, C., and A. Parmigiani (2018), A Physical Model for Three-Phase Compaction in Silicic Magma Reservoirs, *Journal of Geophysical Research: Solid Earth*, *123*(4), 2685-2705.

Huber, C., A. Parmigiani, B. Chopard, M. Manga, and O. Bachmann (2008), Lattice Boltzmann model for melting with natural convection, *International Journal of Heat and Fluid Flow*, *29*(5), 1469-1480, doi:10.1016/j.ijheatfluidflow.2008.05.002.

Hughes, K. G., P. J. Langhorne, G. H. Leonard, and C. L. Stevens (2014), Extension of an Ice Shelf Water plume model beneath sea ice with application in McMurdo Sound, Antarctica, *Journal of Geophysical Research-Oceans*, *119*(12), 8662-8687, doi:10.1002/2013jc009411.

Huguet, L., T. Alboussiere, M. I. Bergman, R. Deguen, S. Labrosse, and G. Lesoeur (2016), Structure of a mushy layer under hypergravity with implications for Earth's inner core, *Geophysical Journal International*, *204*(3), 1729-1755, doi:10.1093/gji/ggv554.

Hunke, E. C., D. Notz, A. K. Turner, and M. Vancoppenolle (2011), The multiphase physics of sea ice: a review for model developers, *Cryosphere*, *5*(4), 989-1009, doi:10.5194/tc-5-989-2011.

Hussmann, H., and T. Spohn (2004), Thermal-orbital evolution of Io and Europa, *Icarus*, *171*(2), 391-410, doi:10.1016/j.icarus.2004.05.020.

Hussmann, H., T. Spohn, and K. Wieczerkowski (2002), Thermal equilibrium states of Europa's ice shell: Implications for internal ocean thickness and surface heat flow, *Icarus*, *156*(1), 143-151, doi:10.1006/icar.2001.6776.

Jaumann, R., R. N. Clark, F. Nimmo, A. R. Hendrix, B. J. Buratti, T. Denk, J. M. Moore, P. M. Schenk, S. J. Ostro, and R. Srama (2009), Icy satellites: Geological evolution and surface processes, in *Saturn from Cassini-Huygens*, edited, pp. 637-681, Springer.

Johnson, B. C., T. J. Bowling, A. J. Trowbridge, and A. M. Freed (2016), Formation of the Sputnik Planum basin and the thickness of Pluto's subsurface ocean, *Geophysical Research Letters*, *43*(19), 10068-10077, doi:10.1002/2016gl070694.

Johnson, B. C., R. Y. Sheppard, A. C. Pascuzzo, E. A. Fisher, and S. E. Wiggins (2017), Porosity and Salt Content Determine if Subduction Can Occur in Europa's Ice Shell, *Journal of Geophysical Research-Planets*, *122*(12), 2765-2778, doi:10.1002/2017je005370.

Jordan, J. S., and M. A. Hesse (2015), Reactive transport in a partially molten system with binary solid solution, *Geochemistry Geophysics Geosystems*, *16*(12), 4153-4177, doi:10.1002/2015gc005956.

Kalousova, K., D. M. Schroeder, and K. M. Soderlund (2017), Radar attenuation in Europa's ice shell: Obstacles and opportunities for constraining the shell thickness and its thermal structure, *Journal of Geophysical Research-Planets*, *122*(3), 524-545, doi:10.1002/2016je005110.

Kalousová, K., O. Souček, G. Tobie, G. Choblet, and O. Čadek (2014), Ice melting and downward transport of meltwater by two-phase flow in Europa's ice shell, *Journal of Geophysical Research: Planets*, *119*(3), 532-549.

Kalousová, K., O. Souček, G. Tobie, G. Choblet, and O. Čadek (2016), Water generation and transport below Europa's strike-slip faults, *Journal of Geophysical Research: Planets*, *121*(12), 2444-2462.

Kargel, J. S., J. Z. Kaye, J. W. Head, G. M. Marion, R. Sassen, J. K. Crowley, O. Prieto Ballesteros, S. A. Grant, and D. L. Hogenboom (2000), Europa's crust and ocean: Origin, composition, and the prospects for life, *Icarus*, *148*(1), 226-265, doi:10.1006/icar.2000.6471.

Kattenhorn, S. A., and T. Hurford (2009), Tectonics of Europa, in *Europa*, edited, pp. 199-236, University of Arizona Press Tucson.

Kattenhorn, S. A., and L. M. Prockter (2014), Evidence for subduction in the ice shell of Europa, *Nature Geoscience*, *7*(10), 762-767, doi:10.1038/Ngeo2245.

Katz, R. F., and M. G. Worster (2008), Simulation of directional solidification, thermochemical convection, and chimney formation in a Hele-Shaw cell, *Journal of Computational Physics*, *227*(23), 9823-9840, doi:10.1016/j.jcp.2008.06.039.

Kawano, Y., and T. Ohashi (2008), Effect of salinity diffusion and heat flux on the growth of sea ice microstructure.

Khazendar, A., and A. Jenkins (2003), A model of marine ice formation within Antarctic ice shelf rifts, *Journal of Geophysical Research-Oceans*, *108*(C7), doi:Artn 3235 10.1029/2002jc001673.

Khazendar, A., E. Rignot, and E. Larour (2009), Roles of marine ice, rheology, and fracture in the flow and stability of the Brunt/Stancomb-Wills Ice Shelf, *Journal of Geophysical Research: Earth Surface*, *114*(F4).

Kivelson, M. G., K. K. Khurana, C. T. Russell, M. Volwerk, R. J. Walker, and C. Zimmer (2000), Galileo magnetometer measurements: A stronger case for a subsurface ocean at Europa, *Science*, *289*(5483), 1340-1343, doi:DOI 10.1126/science.289.5483.1340.

Koenig, L. S., C. Miege, R. R. Forster, and L. Brucker (2014), Initial in situ measurements of perennial meltwater storage in the Greenland firn aquifer, *Geophysical Research Letters*, *41*(1), 81-85, doi:10.1002/2013gl058083.

Korosov, A. A., P. Rampal, L. T. Pedersen, R. Saldo, Y. F. Ye, G. Heygster, T. Lavergne, S. Aaboe, and F. Girard-Ardhuin (2018), A new tracking algorithm for sea ice age distribution estimation, *Cryosphere*, *12*(6), 2073-2085, doi:10.5194/tc-12-2073-2018.

Krembs, C., H. Eicken, and J. W. Deming (2011), Exopolymer alteration of physical properties of sea ice and implications for ice habitability and biogeochemistry in a warmer Arctic, *Proc Natl Acad Sci U S A*, *108*(9), 3653-3658, doi:10.1073/pnas.1100701108.

Kurtz, N. T., and T. Markus (2012), Satellite observations of Antarctic sea ice thickness and volume, *Journal of Geophysical Research-Oceans*, *117*(C8), doi:Artn C08025 10.1029/2012jc008141.

Kuskov, O. L., and V. A. Kronrod (2005), Internal structure of Europa and Callisto, *Icarus*, *177*(2), 550-569, doi:10.1016/j.icarus.2005.04.014.

Lake, R. A., and E. L. Lewis (1970), Salt Rejection by Sea Ice during Growth, *Journal of Geophysical Research*, *75*(3), 583-&, doi:DOI 10.1029/JC075i003p00583.

Langhorne, P., K. Hughes, A. Gough, I. Smith, M. Williams, N. Robinson, C. Stevens, W. Rack, D. Price, and G. Leonard (2015), Observed platelet ice distributions in Antarctic sea ice: An index for ocean-ice shelf heat flux, *Geophysical Research Letters*, *42*(13), 5442-5451.

Laxon, S. W., K. A. Giles, A. L. Ridout, D. J. Wingham, R. Willatt, R. Cullen, R. Kwok, A. Schweiger, J. Zhang, and C. Haas (2013), CryoSat-2 estimates of Arctic sea ice thickness and volume, *Geophysical Research Letters*, *40*(4), 732-737.

Lay, T., J. Hernlund, and B. A. Buffett (2008), Core-mantle boundary heat flow, *Nature Geoscience*, *1*(1), 25-32, doi:10.1038/ngeo.2007.44.

Lewis, E. L., and R. G. Perkin (1983), Supercooling and Energy Exchange near the Arctic Ocean Surface, *Journal of Geophysical Research-Oceans*, *88*(Nc12), 7681-7685, doi:DOI 10.1029/JC088iC12p07681.

Loose, B., W. R. McGillis, P. Schlosser, D. Perovich, and T. Takahashi (2009), Effects of freezing, growth, and ice cover on gas transport processes in laboratory seawater experiments, *Geophysical Research Letters*, *36*(5), doi:Artn L05603 10.1029/2008gl036318.

Loose, B., L. A. Miller, S. Elliott, and T. Papakyriakou (2011), Sea Ice Biogeochemistry and Material Transport Across the Frozen Interface, *Oceanography*, *24*(3), 202-218, doi:DOI 10.5670/oceanog.2011.72.

Lyubetskaya, T., and J. Korenaga (2007), Chemical composition of Earth's primitive mantle and its variance: 2. Implications for global geodynamics, *Journal of Geophysical Research-Solid Earth*, *112*(B3), doi:Artn B03212 10.1029/2005jb004224.

Malmgren, F. (1927), *On the properties of sea-ice*, AS John Griegs Boktrykkeri.

Manga, M., and C. Michaut (2017), Formation of lenticulae on Europa by saucer-shaped sills, *Icarus*, *286*, 261-269, doi:10.1016/j.icarus.2016.10.009.

Manga, M., and A. Sinton (2004), Formation of bands and ridges on Europa by cyclic deformation: Insights from analogue wax experiments, *Journal of Geophysical Research-Planets*, *109*(E9), doi:Artn E09001 10.1029/2004je002249.

Manga, M., and C. Y. Wang (2007), Pressurized oceans and the eruption of liquid water on Europa and Enceladus, *Geophysical Research Letters*, *34*(7), doi:Artn L07202 10.1029/2007gl029297.

Maruyama, S., M. Santosh, and D. Zhao (2007), Superplume, supercontinent, and post-perovskite: Mantle dynamics and anti-plate tectonics on the Core-Mantle Boundary, *Gondwana Research*, *11*(1-2), 7-37, doi:10.1016/j.gr.2006.06.003.

McCarthy, C., J. R. Blackford, and C. E. Jeffree (2013), Low-temperature-SEM study of dihedral angles in the ice-I/sulfuric acid partially molten system, *J Microsc*, *249*(2), 150-157, doi:10.1111/jmi.12003.

McCarthy, C., R. F. Cooper, D. L. Goldsby, W. B. Durham, and S. H. Kirby (2011), Transient and steady state creep response of ice I and magnesium sulfate hydrate eutectic aggregates, *Journal of Geophysical Research-Planets*, *116*(E4), doi:Artn E04007 10.1029/2010je003689.

McCarthy, C., R. F. Cooper, S. H. Kirby, K. D. Rieck, and L. A. Stern (2007), Solidification and microstructures of binary ice-I/hydrate eutectic aggregates, *American Mineralogist*, *92*(10), 1550-1560, doi:10.2138/am.2007.2435.

Mckenzie, D. (1984), The Generation and Compaction of Partially Molten Rock, *Journal of Petrology*, *25*(3), 713-765, doi:DOI 10.1093/petrology/25.3.713.

McKinnon, W. B. (1999), Convective instability in Europa's floating ice shell, *Geophysical Research Letters*, *26*(7), 951-954, doi:Doi 10.1029/1999gl900125.

Melosh, H. J., A. G. Ekholm, A. P. Showman, and R. D. Lorenz (2004), The temperature of Europa's subsurface water ocean, *Icarus*, *168*(2), 498-502, doi:10.1016/j.icarus.2003.11.026.

Meyer, C. R., and B. M. Minchew (2018), Temperate ice in the shear margins of the Antarctic Ice Sheet: Controlling processes and preliminary locations, *Earth and Planetary Science Letters*, *498*, 17-26, doi:10.1016/j.epsl.2018.06.028.

Michaut, C., and M. Manga (2014), Domes, pits, and small chaos on Europa produced by water sills, *Journal of Geophysical Research: Planets*, *119*(3), 550-573.

Mitri, G., and A. P. Showman (2005), Convective-conductive transitions and sensitivity of a convecting ice shell to perturbations in heat flux and tidal-heating rate: Implications for Europa, *Icarus*, *177*(2), 447-460, doi:10.1016/j.icarus.2005.03.019.

Moore, J. C. (2000), Models of radar absorption in Europan ice, *Icarus*, *147*(1), 292-300, doi:DOI 10.1006/icar.2000.6425.

Nagel, K., D. Breuer, and T. Spohn (2004), A model for the interior structure, evolution, and differentiation of Callisto, *Icarus*, *169*(2), 402-412, doi:10.1016/j.icarus.2003.12.019.

Nakagawa, T., and P. J. Tackley (2004), Effects of a perovskite-post perovskite phase change near core-mantle boundary in compressible mantle convection, *Geophysical Research Letters*, *31*(16).

Nakawo, M., and N. K. Sinha (1981), Growth rate and salinity profile of first-year sea ice in the high Arctic, *Journal of Glaciology*, *27*(96), 315-330.

Nimmo, F., et al. (2016), Reorientation of Sputnik Planitia implies a subsurface ocean on Pluto, *Nature*, *540*(7631), 94-96, doi:10.1038/nature20148.

Nimmo, F., and R. T. Pappalardo (2016), Ocean worlds in the outer solar system, *Journal of Geophysical Research-Planets*, *121*(8), 1378-1399, doi:10.1002/2016je005081.

Notz, D. (2012), Challenges in simulating sea ice in Earth System Models, *Wiley Interdisciplinary Reviews-Climate Change*, *3*(6), 509-526, doi:10.1002/wcc.189.

Notz, D., and C. M. Bitz (2017), Sea ice in Earth system models, *Sea ice*, 304-325.

Notz, D., and M. G. Worster (2008), In situ measurements of the evolution of young sea ice, *Journal of Geophysical Research-Oceans*, *113*(C3), doi:Artn C03001 10.1029/2007jc004333.

Oertling, A. B., and R. G. Watts (2004), Growth of and brine drainage from NaCl-H2O freezing: A simulation of young sea ice, *Journal of Geophysical Research: Oceans*, *109*(C4).

Ohashi, T. (2007), Numerical simulation of salinity diffusion and growth instability in the microstructure evolution of sea ice, paper presented at Proceedings of the 22th international symposium on Okhotsk sea & sea ice, 2007.

Ojakangas, G. W., and D. J. Stevenson (1989), Thermal State of an Ice Shell on Europa, *Icarus*, *81*(2), 220-241, doi:Doi 10.1016/0019-1035(89)90052-3.

Olson, P., G. Schubert, and C. Anderson (1987), Plume Formation in the D"-Layer and the Roughness of the Core Mantle Boundary, *Nature*, *327*(6121), 409-413, doi:DOI 10.1038/327409a0.

Olson, P. L., R. S. Coe, P. E. Driscoll, G. A. Glatzmaier, and P. H. Roberts (2010), Geodynamo reversal frequency and heterogeneous core-mantle boundary heat flow, *Physics of the Earth and Planetary Interiors*, *180*(1-2), 66-79, doi:10.1016/j.pepi.2010.02.010.

Pappalardo, R., and M. Coon (1996), A sea ice analog for the surface of Europa, paper presented at Lunar and Planetary Science Conference.

Pappalardo, R. T., and A. C. Barr (2004), The origin of domes on Europa: The role of thermally induced compositional diapirism, *Geophysical Research Letters*, *31*(1), doi:Artn L01701 10.1029/2003gl019202.

Parkinson, J. R., D. F. Martin, A. J. Wells, and R. F. Katz (2020), Modelling binary alloy solidification with adaptive mesh refinement, *Journal of Computational Physics: X*, *5*, 100043.

Perovich, D. K., B. C. Elder, and J. A. RichterMenge (1997), Observations of the annual cycle of sea ice temperature and mass balance, *Geophysical Research Letters*, *24*(5), 555-558, doi:Doi 10.1029/97gl00185.

Perovich, D. K., T. C. Grenfell, B. Light, B. C. Elder, J. Harbeck, C. Polashenski, W. B. Tucker, and C. Stelmach (2009), Transpolar observations of the morphological properties of Arctic sea ice, *Journal of Geophysical Research-Oceans*, *114*(C1), doi:Artn C00a04 10.1029/2008jc004892.

Petrich, C., and H. Eicken (2010), Growth, structure and properties of sea ice, *Sea ice*, *2*, 23-77.

Porco, C. C., et al. (2006), Cassini observes the active south pole of Enceladus, *Science*, *311*(5766), 1393-1401, doi:10.1126/science.1123013.

Postberg, F., S. Kempf, J. Schmidt, N. Brilliantov, A. Beinsen, B. Abel, U. Buck, and R. Srama (2009), Sodium salts in E-ring ice grains from an ocean below the surface of Enceladus, *Nature*, *459*(7250), 1098-1101, doi:10.1038/nature08046.

Postberg, F., J. Schmidt, J. Hillier, S. Kempf, and R. Srama (2011), A salt-water reservoir as the source of a compositionally stratified plume on Enceladus, *Nature*, *474*(7353), 620-622, doi:10.1038/nature10175.

Prockter, L. M. (2017), The Structure and Thickness of Europa's Ice Shell, paper presented at Accessing the Subsurface Oceans of Icy Worlds, California Institute of Technology, October 9-12.

Prockter, L. M., J. W. Head, R. T. Pappalardo, R. J. Sullivan, A. E. Clifton, B. Giese, R. Wagner, and G. Neukum (2002), Morphology of Europan bands at high resolution: A mid-ocean ridge-type rift mechanism, *Journal of Geophysical Research: Planets*, *107*(E5).

Rees Jones, D. W., and M. G. Worster (2013), A simple dynamical model for gravity drainage of brine from growing sea ice, *Geophysical Research Letters*, *40*(2), 307-311.

Reiners, P. W. (1998), Reactive melt transport in the mantle and geochemical signatures of mantle-derived magmas, *Journal of Petrology*, *39*(5), 1039-1061, doi:DOI 10.1093/petrology/39.5.1039.

Robinson, N. J., M. J. M. Williams, C. L. Stevens, P. J. Langhorne, and T. G. Haskell (2014), Evolution of a supercooled Ice Shelf Water plume with an actively growing subice platelet matrix, *Journal of Geophysical Research-Oceans*, *119*(6), 3425-3446, doi:10.1002/2013jc009399.

Robuchon, G., and F. Nimmo (2011), Thermal evolution of Pluto and implications for surface tectonics and a subsurface ocean, *Icarus*, *216*(2), 426-439, doi:10.1016/j.icarus.2011.08.015.

Rubinšteĭn, L. (2000), *The stefan problem*, American Mathematical Soc.

Ruesch, O., et al. (2016), Cryovolcanism on Ceres, *Science*, *353*(6303), aaf4286, doi:10.1126/science.aaf4286.

Schenk, P., et al. (2019), The central pit and dome at Cerealia Facula bright deposit and floor deposits in Occator crater, Ceres: Morphology, comparisons and formation, *Icarus*, *320*, 159-187, doi:10.1016/j.icarus.2018.08.010.

Schmidt, B. (2020), The Astrobiology of Europa and the Jovian System, *Planetary Astrobiology*, 185.

Schmidt, B. E., D. D. Blankenship, G. W. Patterson, and P. M. Schenk (2011), Active formation of 'chaos terrain' over shallow subsurface water on Europa, *Nature*, *479*(7374), 502-505, doi:10.1038/nature10608.

Schmidt, B. E., J. Buffo, and A. Main Campus (2017), Biomarker Production and Preservation on Europa, paper presented at European Planetary Science Congress.

Schubert, G., J. Anderson, T. Spohn, and W. McKinnon (2004), Interior composition, structure and dynamics of the Galilean satellites, *Jupiter: The planet, satellites and magnetosphere*, *1*, 281-306.

Scully, J. E. C., D. L. Buczkowski, C. A. Raymond, T. Bowling, D. A. Williams, A. Neesemann, P. M. Schenk, J. C. Castillo-Rogez, and C. T. Russell (2019), Ceres' Occator crater and its faculae explored through geologic mapping, *Icarus*, *320*, 7-23, doi:10.1016/j.icarus.2018.04.014.

Soderlund, K. M. (2019), Ocean Dynamics of Outer Solar System Satellites, *Geophysical Research Letters*, *46*(15), 8700-8710, doi:10.1029/2018gl081880.

Soderlund, K. M., B. E. Schmidt, J. Wicht, and D. D. Blankenship (2014), Ocean-driven heating of Europa's icy shell at low latitudes, *Nature Geoscience*, *7*(1), 16-19, doi:10.1038/Ngeo2021.

Sohl, F., H. Hussmann, B. Schwentker, T. Spohn, and R. D. Lorenz (2003), Interior structure models and tidal Love numbers of Titan, *Journal of Geophysical Research-Planets*, *108*(E12), doi:Artn 5130 10.1029/2003je002044.

Sotin, C., and G. Tobie (2004), Internal structure and dynamics of the large icy satellites, *Comptes Rendus Physique*, *5*(7), 769-780, doi:10.1016/j.crhy.2004.08.001.

Sparks, W. B., K. P. Hand, M. A. McGrath, E. Bergeron, M. Cracraft, and S. E. Deustua (2016), Probing for Evidence of Plumes on Europa with Hst/Stis, *Astrophysical Journal*, *829*(2), 121, doi:Artn 121 10.3847/0004-637x/829/2/121.

Steefel, C. I., D. J. DePaolo, and P. C. Lichtner (2005), Reactive transport modeling: An essential tool and a new research approach for the Earth sciences, *Earth and Planetary Science Letters*, *240*(3-4), 539-558, doi:10.1016/j.epsl.2005.09.017.

Tedesco, L., and M. Vichi (2014), Sea ice biogeochemistry: a guide for modellers, *PLoS One*, *9*(2), e89217, doi:10.1371/journal.pone.0089217.

Thomas, D. N., and G. S. Dieckmann (2003), Biogeochemistry of Antarctic sea ice, in *Oceanography and Marine Biology, An Annual Review, Volume 40*, edited, pp. 151-156, CRC Press.

Toner, J. D., D. C. Catling, and B. Light (2014), The formation of supercooled brines, viscous liquids, and low-temperature perchlorate glasses in aqueous solutions relevant to Mars, *Icarus*, *233*, 36-47, doi:10.1016/j.icarus.2014.01.018.

Turcotte, D., and G. Schubert (2014), *Geodynamics*, Cambridge University Press.

Turner, A. K., and E. C. Hunke (2015), Impacts of a mushy-layer thermodynamic approach in global sea-ice simulations using the CICE sea-ice model, *Journal of Geophysical Research: Oceans*, *120*(2), 1253-1275.

Turner, A. K., E. C. Hunke, and C. M. Bitz (2013), Two modes of sea-ice gravity drainage: A parameterization for large-scale modeling, *Journal of Geophysical Research: Oceans*, *118*(5), 2279-2294.

Vance, S., M. Bouffard, M. Choukroun, and C. Sotin (2014), Ganymede's internal structure including thermodynamics of magnesium sulfate oceans in contact with ice, *Planetary and Space Science*, *96*, 62-70, doi:10.1016/j.pss.2014.03.011.

Vance, S. D., L. M. Barge, S. S. S. Cardoso, and J. H. E. Cartwright (2019), Self-Assembling Ice Membranes on Europa: Brinicle Properties, Field Examples, and Possible Energetic Systems in Icy Ocean Worlds, *Astrobiology*, *19*(5), 685-695, doi:10.1089/ast.2018.1826.

Vance, S. D., K. P. Hand, and R. T. Pappalardo (2016), Geophysical controls of chemical disequilibria in Europa, *Geophysical Research Letters*, *43*(10), 4871-4879, doi:10.1002/2016gl068547.

Vance, S. D., M. P. Panning, S. Stähler, F. Cammarano, B. G. Bills, G. Tobie, S. Kamata, S. Kedar, C. Sotin, and W. T. Pike (2018), Geophysical investigations of habitability in ice-covered ocean worlds, *Journal of Geophysical Research: Planets*, *123*(1), 180-205.

Vancoppenolle, M., et al. (2013), Role of sea ice in global biogeochemical cycles: emerging views and challenges, *Quaternary Science Reviews*, *79*, 207-230, doi:10.1016/j.quascirev.2013.04.011.

Vancoppenolle, M., and L. Tedesco (2015), Numerical modelling of sea ice biogeochemistry, *Sea Ice*.

Weeks, W., and G. Lofgren (1967), The effective solute distribution coefficient during the freezing of NaCl solutions, *Physics of Snow and Ice: proceedings*, *1*(1), 579-597.

Wells, A. J., J. R. Hitchen, and J. R. G. Parkinson (2019), Mushy-layer growth and convection, with application to sea ice, *Philos Trans A Math Phys Eng Sci*, *377*(2146), 20180165, doi:10.1098/rsta.2018.0165.

Wells, A. J., J. S. Wettlaufer, and S. A. Orszag (2010), Maximal potential energy transport: a variational principle for solidification problems, *Phys Rev Lett*, *105*(25), 254502, doi:10.1103/PhysRevLett.105.254502.

Wells, A. J., J. S. Wettlaufer, and S. A. Orszag (2011), Brine fluxes from growing sea ice, *Geophysical Research Letters*, *38*(4), doi:Artn L04501 10.1029/2010gl046288.

Wettlaufer, J. S. (2010), Sea ice and astrobiology, in *Sea ice*, edited.

Wettlaufer, J. S., M. G. Worster, and H. E. Huppert (1997a), Natural convection during solidification of an alloy from above with application to the evolution of sea ice, *Journal of Fluid Mechanics*, *344*, 291-316, doi:Doi 10.1017/S0022112097006022.

Wettlaufer, J. S., M. G. Worster, and H. E. Huppert (1997b), The phase evolution of young sea ice, *Geophysical Research Letters*, *24*(10), 1251-1254, doi:Doi 10.1029/97gl00877.

Wettlaufer, J. S., M. G. Worster, and H. E. Huppert (2000), Solidification of leads: Theory, experiment, and field observations, *Journal of Geophysical Research-Oceans*, *105*(C1), 1123-1134, doi:Doi 10.1029/1999jc900269.

Wolfenbarger, N., D. Blankenship, K. Soderlund, D. Young, and C. Grima (2018), Leveraging Terrestrial Marine Ice Cores to Constrain the Composition of Ice on Europa, *LPI Contributions*, *2100*.

Wolfenbarger, N., K. Soderlund, and D. Blankenship (2019), Revisiting the Salt Distribution Coefficient for Icy Ocean Worlds, *LPI Contributions*, *2168*.

Wongpan, P., P. J. Langhorne, D. E. Dempsey, L. Hahn-Woernle, and Z. F. Sun (2015), Simulation of the crystal growth of platelet sea ice with diffusive heat and mass transfer, *Annals of Glaciology*, *56*(69), 127-136, doi:10.3189/2015AoG69A777.

Worster, M. G. (1986), Solidification of an Alloy from a Cooled Boundary, *Journal of Fluid Mechanics*, *167*, 481-501, doi:Doi 10.1017/S0022112086002938.

Worster, M. G., H. E. Huppert, and R. S. J. Sparks (1990), Convection and Crystallization in Magma Cooled from Above, *Earth and Planetary Science Letters*, *101*(1), 78-89, doi:Doi 10.1016/0012-821x(90)90126-I.

Worster, M. G., and D. W. Rees Jones (2015), Sea-ice thermodynamics and brine drainage, *Philos Trans A Math Phys Eng Sci*, *373*(2045), 20140166, doi:10.1098/rsta.2014.0166.

Zhong, J. Q., A. T. Fragoso, A. J. Wells, and J. S. Wettlaufer (2012), Finite-sample-size effects on convection in mushy layers, *Journal of Fluid Mechanics*, *704*, 89-108, doi:10.1017/jfm.2012.219.

Zhong, S., A. McNamara, E. Tan, L. Moresi, and M. Gurnis (2008), A benchmark study on mantle convection in a 3-D spherical shell using CitcomS, *Geochemistry, Geophysics, Geosystems*, *9*(10).

Zolotov, M. Y., E. Shock, A. Barr, and R. Pappalardo (2004), Brine pockets in the icy shell on Europa: Distribution, chemistry, and habitability.

Zolotov, M. Y., and E. L. Shock (2001), Composition and stability of salts on the surface of Europa and their oceanic origin, *Journal of Geophysical Research-Planets*, *106*(E12), 32815-32827, doi:Doi 10.1029/2000je001413.
Zotikov, I. A., V. S. Zagorodnov, and J. V. Raikovsky (1980), Core Drilling through the Ross Ice Shelf (Antarctica) Confirmed Basal Freezing, *Science*, *207*(4438), 1463-1464, doi:DOI 10.1126/science.207.4438.1463.

Supplementary Material

J. J. Buffo[1], B. E. Schmidt[2], C. Huber[3], C. R. Meyer[1]
[1]Dartmouth College, [2]Georgia Institute of Technology, [3]Brown University

Contained below are three supplementary material sections which support and/or provide additional detail to the work and conclusions presented in the main manuscript: *Characterizing the Ice-Ocean Interface of Icy Worlds: A Theoretical Approach*. Section S1 provides the complete solution to the molecular diffusion equation in the mushy layer – as outlined in Section 2.1.1 of the main text. Section S2 provides a table of all variables used throughout the text as well as their associated symbols and units. Finally, Section S3 provides a table of the ionic species present and their relative abundances in the terrestrial ocean composition we assume throughout the investigation.

S1. Solving the Molecular Diffusion Equation

The evolution of salinity at the ice-mush interface is governed by:

$$\frac{\partial S}{\partial t} = D\frac{\partial^2 S}{\partial z^2} \qquad (S1)$$

Utilizing the similarity variable $\eta = z/2\sqrt{Dt}$ and boundary conditions (Equations 9-10) it can be shown that:

$$\theta = \frac{1}{erfc(\lambda_S)} - \frac{\operatorname{erf}(\eta)}{erfc(\lambda_S)} \qquad (S2)$$

Writing in terms of the original variables *S, z* and *t*:

$$S = S_{oc} + (S_{int} - S_{oc})\left(\frac{1}{erfc(\lambda_S)} - \frac{\operatorname{erf}\left(z/2\sqrt{Dt}\right)}{erfc(\lambda_S)}\right) \qquad (S3)$$

The Stefan condition for this problem can be garnered from the equation for conservation of salt (no salt in the ice phase):

$$\int_{z_m^*(t)}^{\infty} S(z,t)dz = cnst. \qquad (S4)$$

Taking the temporal derivative of this equation and applying the Leibniz integral rule:

$$-S(z_m^*, t)\frac{dz_m^*}{dt} + \int_{z_m^*(t)}^{\infty} \frac{\partial S}{\partial t}dz = 0 \qquad (S5)$$

Substituting $\frac{\partial S}{\partial t} = D\frac{\partial^2 S}{\partial z^2}$, noting $S(z_m^*, t) = S_{int}$ and carrying out the integral gives:

$$S_{int}\frac{dz_m^*}{dt} = -D\frac{\partial S(z = z_m^*)}{\partial z} \qquad (S6)$$

The derivatives are:

$$\frac{dz_m^*}{dt} = \frac{\lambda_S\sqrt{D}}{\sqrt{t}} \qquad (S7)$$

And

$$\frac{\partial S(z = z_m^*)}{\partial z} = \frac{-(S_{int} - S_{oc})}{erfc(\lambda_S)}\frac{\exp\left(-\lambda_S^2\right)}{\sqrt{\pi Dt}} \qquad (S8)$$

Substituting back into Equation 17,

$$S_{int}\sqrt{\pi} = \frac{(S_{int} - S_{oc})}{\lambda_S erfc(\lambda_S)} \exp(-\lambda_S^2) \qquad (S9)$$

Or, rearranging

$$\lambda_S erfc(\lambda_S) \exp(\lambda_S^2) = \frac{(S_{int} - S_{oc})}{S_{int}\sqrt{\pi}} \qquad (S10)$$

We assume that the interface is at its melting temperature, T_f, which we take as a linear function of salinity $T_f = T_{mp} - 0.066178S$, where T_{mp} is the melting temperature of pure ice and the freezing point depression coefficient has units of K kg g^{-1}. Solving for S and letting T_f lie on a conductive (linear) thermal profile $T(z) = T_S + z(T_{oc} - T_S)/H$ at a depth *H-h*. We have:

$$S_{int} = 15.1106(T_{mp} - T_f) = 15.1106\left(T_{mp} - \left(T_S + (H-h)\frac{(T_{oc} - T_S)}{H}\right)\right) \qquad (S11)$$

Substituting the value of S_{int} into Equation 21 and setting the interface velocities equal ($\dot{z}_m^* = 2\lambda_S\sqrt{D}/\sqrt{t} = 2\lambda_T\sqrt{\kappa_i}/\sqrt{t} = \dot{z}_m$) produces two equations:

$$\lambda_S = \frac{\lambda_T\sqrt{\kappa_i}}{\sqrt{D}} \qquad (S12)$$

and

$$15.1106\left(T_{mp} - \left(T_S + (H-h)\frac{(T_{oc}-T_S)}{H}\right)\right)\sqrt{\pi} = \frac{15.1106\left(T_{mp} - \left(T_S + (H-h)\frac{(T_{oc}-T_S)}{H}\right)\right) - S_{oc}}{\lambda_S erfc(\lambda_S)} \exp(-\lambda_S^2) \qquad (S13)$$

which can be solved for *h*. The equation is linear in *h*, so has one solution.

Archie's law is employed to estimate the molecular diffusion in a porous medium and it is assumed that transport processes (diffusion and advection) will be limited by the critical porosity of ocean/brine derived ices ($\phi_c = 0.05$ [*K M Golden et al.*, 2007]):

$$D = k_S\phi_c^m \qquad (S14)$$

Where k_S is the molecular diffusivity of salt in water and *m* is a cementation exponent, here=2, which describes how ion transport is limited by porosity.

S2. Variables Used in the Text

Symbol	Definition	Units
$\boldsymbol{\alpha}$	1D Advection Coefficient	kg m^{-3} s^{-1}
$\boldsymbol{\beta}$	Density (Salinity) Coefficient	ppt^{-1}
$\boldsymbol{br}^{\uparrow,\downarrow}$	Vertical Brine Velocity	m s^{-1}
$\boldsymbol{c_i}$	Ice Heat Capacity	J kg^{-1} K^{-1}
$\boldsymbol{D}$	Salt Diffusivity	m^2 s^{-1}
$\boldsymbol{\eta}$	Similarity Variable	-
$\boldsymbol{\eta_m}$	Similarity Variable at z_m^*	-
$\boldsymbol{\Gamma}$	Freezing Point Depression Coefficient	K kg g^{-1}
$\boldsymbol{g}$	Acceleration Due to Gravity	m s^{-2}
$\boldsymbol{G}$	Thermal Gradient	K m^{-1}
$\boldsymbol{G'}$	Thermal Gradient Perturbation	K m^{-1}
$\boldsymbol{h}$	Mushy Layer Equilibrium Thickness	m
$\boldsymbol{h'}$	Thickness Perturbation	m
$\boldsymbol{H}$	Ice Shell Thickness	m
$\boldsymbol{k_s}$	Salt Diffusivity in Pure Water	m^2 s^{-1}
$\boldsymbol{\kappa_i}$	Thermal Diffusivity of Ice	m^2 s^{-1}
$\boldsymbol{\kappa_{br}}$	Thermal Diffusivity of Brine	m^2 s^{-1}
$\boldsymbol{L}$	Latent Heat of Fusion	J kg^{-1}
$\boldsymbol{Le}$	Lewis Number	-
$\boldsymbol{\lambda_T}, \boldsymbol{\lambda_S}$	Stefan Problem Variables	-
$\boldsymbol{m}$	Cementation Exponent	-
$\boldsymbol{\mu}$	Kinematic Viscosity	m^2 s^{-1}
$\boldsymbol{\phi}$	Liquid Fraction	-
$\boldsymbol{\phi_c}$	Critical Porosity	-
$\boldsymbol{\Pi}$	Permeability	m^2
$\boldsymbol{Ra_c}$	Critical Rayleigh Number	-
$\boldsymbol{\rho_{sw}}$	Ocean Density	kg m^{-3}
$\boldsymbol{S}$	Salinity	ppt
$\boldsymbol{S_{int}}$	Interface Salinity	ppt
$\boldsymbol{S_{oc}}$	Ocean Salinity	ppt
$\Delta\boldsymbol{S_j}$	$S_{int} - S_{oc}$	ppt
$\boldsymbol{t}$	Time	s
$\boldsymbol{T}$	Temperature	K
$\boldsymbol{T_m}$	Melting/Freezing Temperature	K
$\boldsymbol{T_{oc}}$	Ocean Temperature	K
$\boldsymbol{T_s}$	Surface Temperature	K
$\boldsymbol{\theta}$	Dimensionless Salinity	-
$\boldsymbol{v_m}$	Mush-Ocean Freezing Front Velocity	m s^{-1}
$\boldsymbol{v_m^*}$	Ice-Mush Freezing Front Velocity	m s^{-1}
$\Delta\boldsymbol{V}$	$v_m - v_m^*$	m s^{-1}
$\boldsymbol{z}$	Vertical Coordinate	m
$\boldsymbol{z_m}$	Mush-Ocean Interface	m
$\boldsymbol{z_m^*}$	Ice-Mush Interface	m

S3. Terrestrial Ocean Composition

Species	Terrestrial Seawater (mol/kg)
Na^{+}	4.69×10^{-1}
K^{+}	1.02×10^{-2}
Ca^{2+}	1.03×10^{-2}
Mg^{2+}	5.28×10^{-2}
Cl^{-}	5.46×10^{-1}
SO_4^{2-}	2.82×10^{-2}
Total Salt (ppt)	34

Table S1 – Ocean composition. List of ion species and relative abundances for terrestrial seawater [*Dickson and Goyet*, 1994].